REPORT DOCUMENTATION PAGE

Form Approved
OMB No. 0704-0188

1. REPORT DATE *(DD-MM-YYYY)* 05-10-2013	2. REPORT TYPE	3. DATES COVERED *(From - To)*

4. TITLE AND SUBTITLE	5a. CONTRACT NUMBER
Study of Passive Flow Control for Ship Air Wakes	5b. GRANT NUMBER
	5c. PROGRAM ELEMENT NUMBER

6. AUTHOR(S) LaSalle, Nicholas Robert	5d. PROJECT NUMBER
	5e. TASK NUMBER
	5f. WORK UNIT NUMBER

7. PERFORMING ORGANIZATION NAME(S) AND ADDRESS(ES)	8. PERFORMING ORGANIZATION REPORT NUMBER

9. SPONSORING / MONITORING AGENCY NAME(S) AND ADDRESS(ES) U.S. Naval Academy Annapolis, MD 21402	10. SPONSOR/MONITOR'S ACRONYM(S)
	11. SPONSOR/MONITOR'S REPORT NUMBER(S) Trident Scholar Report no. 418 (2013)

12. DISTRIBUTION / AVAILABILITY STATEMENT

This document has been approved for public release; its distribution is UNLIMITED.

13. SUPPLEMENTARY NOTES

14. ABSTRACT

This Trident project expands ongoing ship air wake research being conducted at the United States Naval Academy (USNA). The objective of this project is to examine the effects of passive flow control techniques aimed at reducing the impact of ship air wakes on naval rotary wing aircraft flight operations. Helicopter flight operations on destroyers and cruisers are limited to specific flight envelopes to ensure the safety of the pilot and aircraft. These flight envelopes are developed based upon helicopter operating capabilities and the impact of air wakes on the aircraft. Modifying the size, shape, and turbulent flow structures of a ship air wake could allow for more expansive helicopter flight envelopes. For this Trident project, a solid, notched fence was placed along the top and sides of the YP hangar, angled aft by 30 degrees, and along the starboard flight deck, angled out board by 30 degrees. Air wake data for this configuration was measured with underway *in situ* testing, computational fluid dynamics (CFD) simulations, and wind tunnel scale model experiments to provide a complete analysis of the effects of the fences on the YP's air wake. This investigation showed that this particular passive flow control fence may produce a less favorable ship air wake for helicopter launch and recovery operations due to an increase in shear, turbulent kinetic energy density, and mixing within the helicopter landing region.

15. SUBJECT TERMS
ship air wake, passive flow control

16. SECURITY CLASSIFICATION OF:			17. LIMITATION OF ABSTRACT	18. NUMBER OF PAGES	19a. NAME OF RESPONSIBLE PERSON
a. REPORT	b. ABSTRACT	c. THIS PAGE		93	19b. TELEPHONE NUMBER *(include area code)*

Standard Form 298 (Rev. 8-98)
Prescribed by ANSI Std. Z39.18

A TRIDENT SCHOLAR
PROJECT REPORT

No. 418

Study of Passive Flow Control For Ship Air Wakes

by

Midshipman 1/C Nicholas R. LaSalle, USN

UNITED STATES NAVAL ACADEMY
ANNAPOLIS, MARYLAND

USNA 1531-2

U.S.N.A. --- Trident Scholar project report; no. 418 (2013)

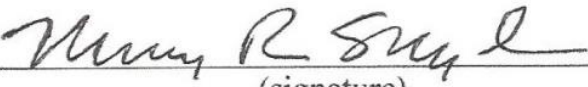**Study of Passive Flow Control for Ship Air Wakes**

by

Midshipman 1/C Nicholas R. LaSalle
United States Naval Academy
Annapolis, Maryland

_____
(signature)

Certification of Adviser(s) Approval

Captain Murray R. Snyder, USN (Retired)
Research Professor, Aerospace Engineering Department

_____
(signature)
3 May 2013
(date)

Dr. Hyung S. Kang
Johns Hopkins, Applied Physics Laboratory

_____
(signature)
5 May 2013
(date)

Acceptance for the Trident Scholar Committee

Professor Maria J. Schroeder
Associate Director of Midshipman Research

_____
(signature)
_____
(date)

USNA-1531-2

A b s t r a c t

This Trident project expands ongoing ship air wake research being conducted at the United States Naval Academy (USNA). The objective of this project is to examine the effects of passive flow control techniques aimed at reducing the impact of ship air wakes on naval rotary wing aircraft flight operations. Helicopter flight operations on destroyers and cruisers are limited to specific flight envelopes to ensure the safety of the pilot and aircraft. These flight envelopes are developed based upon helicopter operating capabilities and the impact of air wakes on the aircraft. Modifying the size, shape, and turbulent flow structures of a ship air wake could allow for more expansive helicopter flight envelopes.

For this Trident project, a solid, notched fence was placed along the top and sides of the YP hangar, angled aft by 30 degrees, and along the starboard flight deck, angled out board by 30 degrees. Air wake data for this configuration was measured with underway *in situ* testing, computational fluid dynamics (CFD) simulations, and wind tunnel scale model experiments to provide a complete analysis of the effects of the fences on the YP's air wake. For a Beta 0 degree headwind condition the fences increased the size of the recirculation zone and produced higher turbulent kinetic energy and more turbulent mixing at the center of the flight deck. For a Beta 15 degree crosswind condition, the fences did not cause a significant change to shear, mixing, or turbulent kinetic energy of the air wake. This investigation showed that this particular passive flow control fence may produce a less favorable ship air wake for helicopter launch and

recovery operations due to an increase in shear, turbulent kinetic energy density, and mixing within the helicopter landing region.

Acknowledgements

4

Table of Contents

List of Figures

List of Tables

List of Symbols

CCWT .... closed circuit wind tunnel
CFD .... computational fluid dynamics
DDG .... guided missile destroyer
ESP .... electronically scanned pressure
NAVAIR .... Naval Air Systems Command
USNA .... United States Naval Academy
WISP .... wake interactive survey probe
YP .... Patrol craft, training
H .... hangar height
x .... distance aft of hangar face
y .... distance starboard of centerline
z .... distance above flight deck surface
u .... x-component of velocity
v .... y-component of velocity
w .... z-component of velocity
u_{rms}, v_{rms}, w_{rms} .... root-mean-squared velocities in x, y, and z directions
α .... flow pitch angle
β .... flow yaw angle
δ .... probe bias error

ω……………………vorticity

1 Introduction

Launch and recovery of naval rotary wing aircraft is a challenging and potentially dangerous activity, but it is vital to several of the Navy's mission areas. Helicopter flight operations are performed on a wide variety of ship classes, but they are often limited by the rapidly changing flow conditions created by ship motion, air turbulence created by the superstructure, and the dynamic interaction of the vessel's air wake and the rotor wake. The eddies and velocity gradients that develop within a ship air wake can impose aerodynamic forces on a helicopter, making launch and recovery operations a more difficult and potentially dangerous evolution.

To ensure the safety of the aircraft, ship, and crew, launch and recovery envelopes have been developed for each aircraft and ship class pairing. Figure 1 shows the acceptable relative wind over deck directions and speeds for safe flight operations aboard Ticonderoga Class cruisers [1]. These flight envelopes are initially very restrictive but are expanded over time by at sea flight testing. During testing, test pilots subjectively analyze the launch and recovery procedures in a variety of ship movement conditions in order to determine if the average fleet pilot would be able to safely operate the aircraft. This testing is often difficult to schedule, expensive, and potentially hazardous for pilots and crew. The risk and cost associated with *in situ* flight testing could possibly be mitigated by the use computational simulations. Accurate simulations could predict flight conditions and generate acceptable approach patterns, thereby reducing the number of at sea flights test required to determine safe operating limits. However,

current computational tools are insufficiently validated to use as a standalone investigation

technique for ships with complicated superstructures such as a cruiser or destroyer [2] – [5].
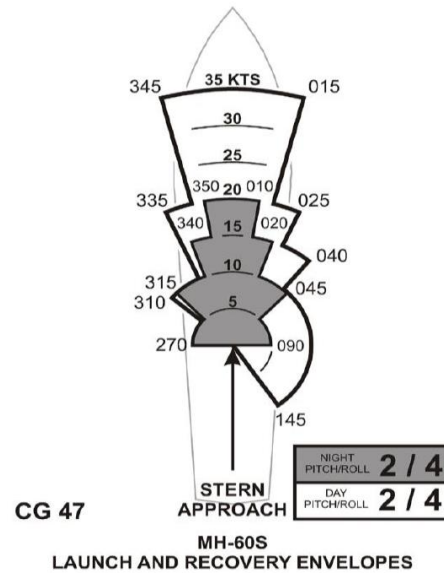
Figure 1. Launch and recovery flight envelope for MH-60S helicopter and USS Ticonderoga
(CG-47) [1]

1.1 Ship Air Wake Project

The Ship Air Wake Project is an ongoing research program at USNA. The project seeks

to develop validated computational fluid dynamics (CFD) tools with the intent of reducing the

necessity of at-sea flight testing, in order to create less expensive and safer methods of

determining helicopter launch and recovery flight envelopes. The CFD results are validated by

additional testing including scale model wind tunnel testing and at-sea *in situ* measurements

using YP's. The unique resources available at USNA allow for a detailed analysis of ship air

wake phenomenon. The Ship Air Wake Project is funded by the Office of Naval Research and

coordinates with related investigation done by Naval Air Systems Command (NAVAIR).

USNA operates a fleet of YPs for midshipmen training. These vessels are relatively large, with a length of 108 ft and an above water-line height of 24 ft, and have a superstructure and deck configuration similar to that of a modern cruiser or destroyer. The size of the YPs allows for testing with a Reynolds number within the same order of magnitude as a modern warship. (Reynolds number is the ratio of inertia to viscous forces and is the most commonly referenced parameter in aeronautical investigations). YP 676 has been modified to include a hangar and flight deck structure that closely resembles a cruiser or destroyer. Figure 2 shows the flight deck and hangar structure of YP 676 used for testing.

Figure 2. Flight deck and hangar of YP 676

Numerical simulations have been conducted by USNA midshipmen using both Cobalt, a commercial CFD code, and Kestrel, a Department of Defense CFD code. Simulations have been performed for various wind over deck velocities and starboard crosswind angles relative to the bow of the ship.

   In situ measurements aboard YP 676 and wind tunnel measurements have also been

collected over the past four years to create a data base of ship air wakes measurements that can

be used for validation of numerical simulations. Air wake flow measurements on YP 676 are

collected using ultrasonic anemometers. Wind tunnel data are collected in the USNA Closed

Circuit Wind Tunnel (CCWT) using a 4% scale model of YP 676.

1.2   Air Wake Flow Physics

   A simplified model for a ship air wake downstream of a hangar structure is a two

dimensional flow over a backward facing step. Figure 3 shows the recirculation zone and

unsteady shear layer that develops downstream of the step. The turbulent flow structures decay

as they move downstream and the flow eventually reattaches to the flight deck surface. This

flow model is relevant to ship board helicopter operations because the air wake flow structures

shown in Figure 3 dominate the helicopter landing region.
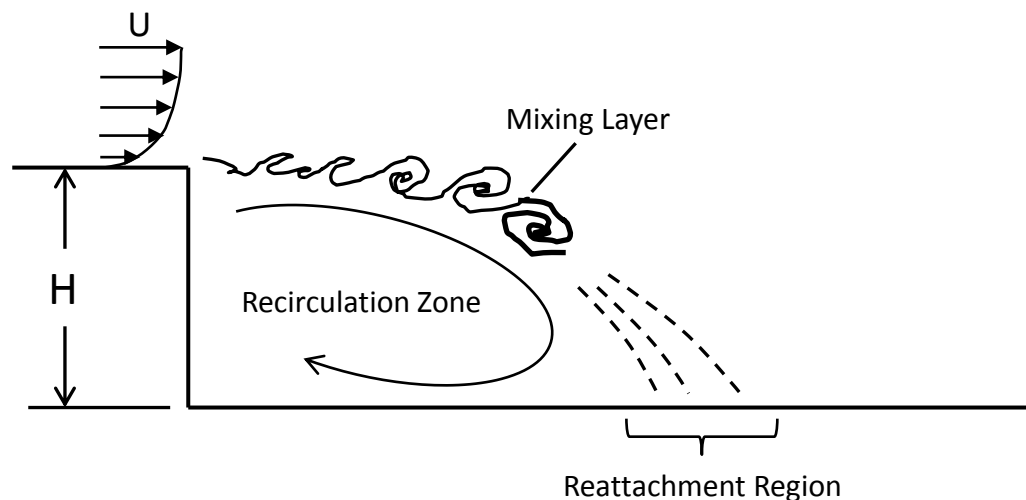
Figure 3. Two dimensional flow over a backwards facing step (recreated from figure in
Reference [6])

The two dimensional backward facing step models are not sufficient to accurately model the flow field for a three dimensional ship. Three dimensional ship hangars produce a horseshoe vortex structure due to the contribution of flow from the sides of the hangar [7]-[9]. The flow field, vortex intensity, and reattachment point change dynamically with vortex shedding from the ship's hangar and superstructure.

1.3   Passive Flow Control

Passive flow control devices are a possible solution for managing a ship's air wake. These devices can be placed into two categories: moving and deflecting flow structures away from the helicopter landing region and modifying the dominant flow structures of the air wake. Moving and deflecting the flow functions to push the recirculation zone and shear layer away from the helicopter operating region. Passive devices that may move or deflect the flow include columnar vortex generators, turning vanes, ramps, and fences. Passive devices that modify flow structures look to change the length scales of the turbulence present in wake or change the amount of mixing present in the helicopter landing region. These devices include porous ship surfaces, vortex generators, and wedges. It is also feasible to use devices that fall into both categories and aim to move the flow and modify the turbulent structures. These devices include porous fences, serrated fences, notched fences, and reticulated foam fences.

Figure 4 shows passive flow control devices that include porous ship surfaces (models 1 and 2), vortex generators (model 3), lateral wedges (model 4), and various fence and turning vane concepts (models 5-14).
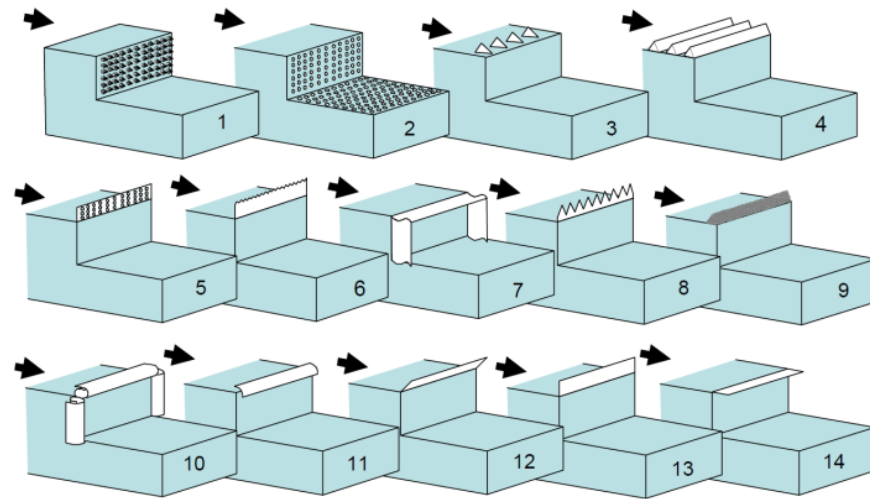
Figure 4. Passive flow control devices [10]

The devices shown in Figure 4 were placed on a scale model of the DDG 81ship and tested in the NAVAIR wind tunnel in Patuxent River, MD. This study by Shafer [10] showed that reticulated foam fences produced the most favorable results by causing the greatest reduction in velocity downstream of the hangar with only a mild increase in velocity fluctuation level near the top of the fence. Although reticulated foam fences produced favorable results in Shaffer's study, their applicability to fleet operations may be limited. Reticulated foam structures would be difficult to maintain on an operational ship due to exposure in a maritime environment and daily shipboard evolutions. In addition, reticulated foam is extremely difficult and unrealistically expensive to model computationally.

Shaffer's study tested a series of notched fences that were both upright and angled upstream into the flow. The investigation found that upright fences created mean velocity reductions over the flight deck but larger velocity gradients above and to the sides of the helicopter landing area. Notched fences increased velocity fluctuation levels at the height of the

fences. Notched fences oriented upstream helped decrease flow unsteadiness but no longer shielded the helicopter landing region, creating a lower mean velocity region [10].

Additional passive flow control research has shown that aft facing screens may be viable solutions for improving a ship air wake for ship board launch and recovery operations. Greenwell and Barrett showed that flow control may become more important at crosswind angles rather than simply just a headwind configuration [11].

1.4   Passive Flow Control Device Selection

A solid notched fence angled downstream was chosen for this investigation. Figure 5 shows a three view drawing of the fence design. Solid fences were chosen because it is difficult to simulate porous surfaces and screens computationally and this investigation required the use of numerical simulations. Angling the fence aft would hopefully shield the helicopter landing region to produce a more favorable velocity gradient downstream of the hangar, while also altering the level of turbulent mixing within the flow. The fences were angled aft/outboard by 30 degrees and each triangle's height was 30% of the height of the YP's hangar. The fence height was chosen as a median value of previous research that had investigated fences ranging from 0.25H to 0.5H [12]-[13], where H is the height of hangar above the flight (59 inches for YP 676). Fences were placed on the top and sides of the ship's hangar and the starboard side of the flight deck in an effort to modify the flow in crosswinds from the starboard side.
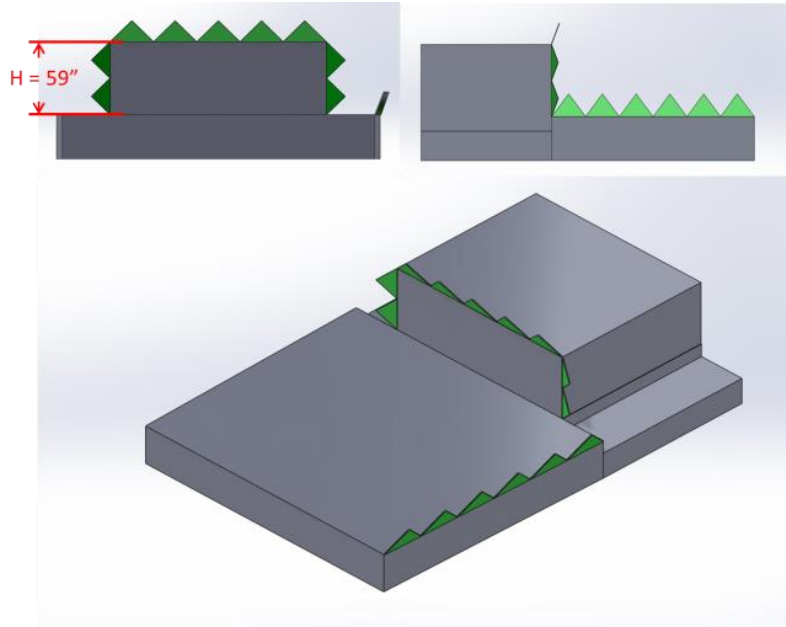
Figure 5. Passive flow control device for this investigation

2 Equipment and Measurement Procedures

2.1 *In situ* measurements

2.1.1 YP 676

In situ testing was performed onboard YP 676, which is dedicated to data collection for the Ship Air Wake Project. YP 676 is 108 feet long and has an above waterline height of 24 feet. YP 676 was modified by adding a hangar structure and flight deck on the fantail of the vessel in order to more closely resemble a cruise or destroyer. Reynolds numbers can be matched within the same order of magnitude for YP's and modern naval warships.

Flow control fences for YP 676 were created from ¾ inch thick marine grade plywood. The fences were mounted to the ship using 1/8 inch thick aluminum brackets bent to create the proper installation angle. The wedges were painted blue to contrast with the ship.

2.1.2 Instrumentation

Ultrasonic anemometers are used to collect air wake velocity measurements on the YP. The anemometers are the Applied Technology Inc. "A" style three-velocity component model with a 5.91 inch path length and a measurement accuracy of ±1.18 inches/sec. They sample at up to 20 Hz and are connected to a data synchronizer that can handle up to 8 individual inputs. Anemometers are mounted on poles fixed to the flight deck. Mounting brackets are affixed to the poles at various heights to achieve desired test points. There are 13 pole mounting locations drilled on the flight deck, and anemometers can be positioned on each individual pole to sample 22 unique test heights at three adjacent test locations.

For this investigation, one anemometer was placed on the bow of the YP to serve as a reference for the incoming flow. The reference anemometer was mounted 3.5 ft forward and 7.0 ft above the ship's bow because CFD simulations suggested this location would have minimal disturbance to the incoming flow due to the ship's hull and superstructure. A display on the bridge of the ship showed the reference wind direction and relative angle from the bow reference anemometer so the helmsman could adjust for fluctuations in wind direction.

2.1.3 Procedure

Underway testing was performed for the $\beta = 0°$ headwind and $\beta = 15°$ crosswind conditions. The sampling locations for each wind angle were chosen based on previous underway data without the flow control fences installed. $\beta = 0°$ testing focused on six planes perpendicular to the *x*-axis at $x/H = 0.492, 1.076, 1.585, 2.169, 2.691$, and 3.275. Within each plane, the air wake was sampled at two lateral flight deck locations, $y/H = 0$ and 0.585. Each test location was sampled at various heights in order to match previous ship air wake underway test points as well as collect data at any points of interest such as the boundary of the recirculation zone or the reattachment point. Test heights ranged from $[z/H]_{min} = 0.15$ to $[z/H]_{max} = 1.41$. $\beta = 15°$ testing used the same test locations but expanding the sampling area to include additional lateral flight deck locations. These locations were $y/H = -1.17, -0.585, 0, 0.585, 1.17$, and 1.75.

For *in situ* testing, up to four anemometers were used to sample the air wake over the flight deck at any one time, and an additional anemometer was mounted on the bow to serve as a reference. All anemometers sampled at 10 Hz. The reference anemometer measured relative wind angle, and its output was displayed on the bridge of the ship to assist the helmsman in

maintaining the desired relative wind angle. Each underway lasted approximately 6-8 hours with

6-7 data runs per underway. Individual runs lasted for 25-30 minutes, providing an average of

10-15 minutes of useful data within ±5 degrees of the desired test condition.

During the underway testing that took place from September 2013 to February 2014, the

reference bow anemometer had to be changed three times because of equipment malfunctions.

This is important to note because *in situ* data is normalized by the average magnitude of the bow

reference velocity for each run. The point x/H = 1.59, y/H = 0, and z/H = 1.21 can be used to

compare the different reference anemometers because this location was sampled five times from

October 2012 to February 2013 and has velocity data normalized by all three bow reference

anemometers. The largest normalized velocity magnitude difference recorded between the five

samples was 3.7%, based on the original reference anemometer. Given this result, it was

concluded that the different bow anemometers would not have a significant impact on the overall

determination of the ship air wake. No scaling was performed on the data to account for

normalization differences due to the different bow anemometers.

Furthermore, previous Ship Air Wake Project research has demonstrated the repeatability

of normalized *in situ* measurements [14]. Therefore, data taken across the five consecutive

months of testing can be satisfactorily compared.

2.2   Computational Fluid Dynamics

Numerical simulations were performed with Cobalt which uses an unstructured tetrahedral

grid. An unstructured grid allows for finer resolution near boundaries and other regions where

complicated flow structures are expected.   The unstructured grid was partitioned to allow for

parallel processing to help reduce computational time. This investigation used a Monotone

Integrated Large Eddy Simulation (MILES), which is a laminar, time accurate flow model. The

MILES approach has correctly determined dominant frequencies within an LHA class US Navy

ship's air wake flow field based on comparison with *in* situ results and wind tunnel testing [15].

Simulations were performed using the Air Force Research Laboratory's Raptor High

Performance Computing system. The flow control fences were added to the preexisting digital

YP model and a new surface grid was generated. Figure 6 shows the updated geometry and

surface grid.
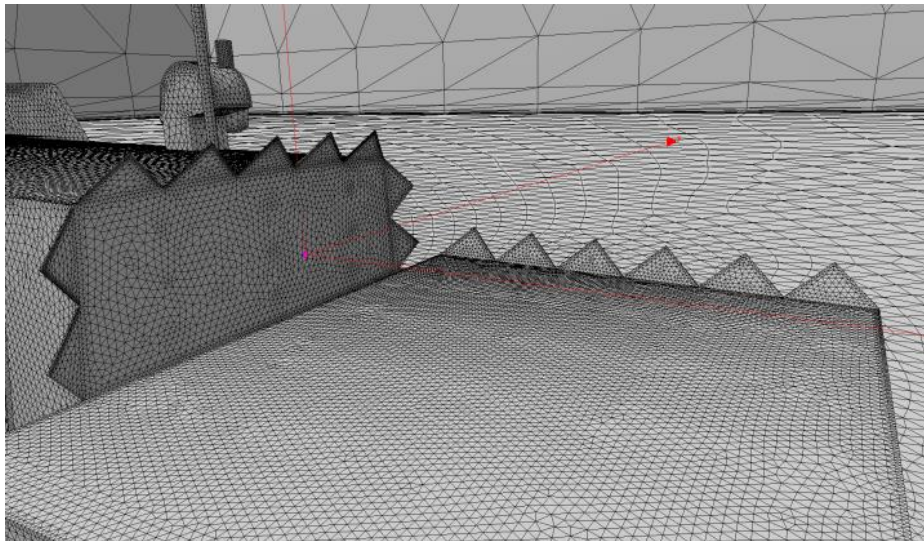
Figure 6. YP surface grid with flow control fences

Simulations were run with 7 and 20 knot inflows for both a headwind condition ($\beta = 0°$)

and a 15° crosswind from the starboard bow ($\beta = 15°$). The simulations used an unstructured

grid of approximately 17 million tetrahedrons. Grid sensitivity studies had been previously

performed that show that 17 million tetrahedrons provided adequate resolution [16].   For the

purposes of comparison, CFD results for the original YP geometry without flow control fences

were available in a database at USNA from previous research performed by the Ship Air Wake project. All numerical simulations used for this investigation were run with a uniform boundary layer inflow.

2.3 Wind Tunnel

The USNA Closed Circuit Wind Tunnel (CCWT) is a single return wind tunnel. The test section is 60 inches wide, 42 inches tall and 120 inches long. The tunnel can achieve a maximum Reynolds number of 1.9 x 10^6 per foot at a maximum velocity of 310 feet per second. An active cooling system regulates test section temperatures at high velocities.

The model for this experiment is a 4% scale model of YP 676. The model is 52.50 inches long and has the same hangar structure found on YP 676. The hangar is 2.361 inches tall, and the flight deck is 8.78 inches long. The ship model includes every detail from the full size ship that is approximately 2 inches or larger. These features include the mast, ladders, hatch covers, capstans, vents, and lights.

For the purposes of studying passive flow control, sheet metal fences were added to the hangar and flight deck of the YP model. The fences were constructed of 1/16 inch thick aluminum sheet metal and fastened to the model using wood screws. Aluminum tape was used to create a smooth surface over the screw heads. Figure 7 shows the YP model mounted in the CCWT with the flow control fences installed.
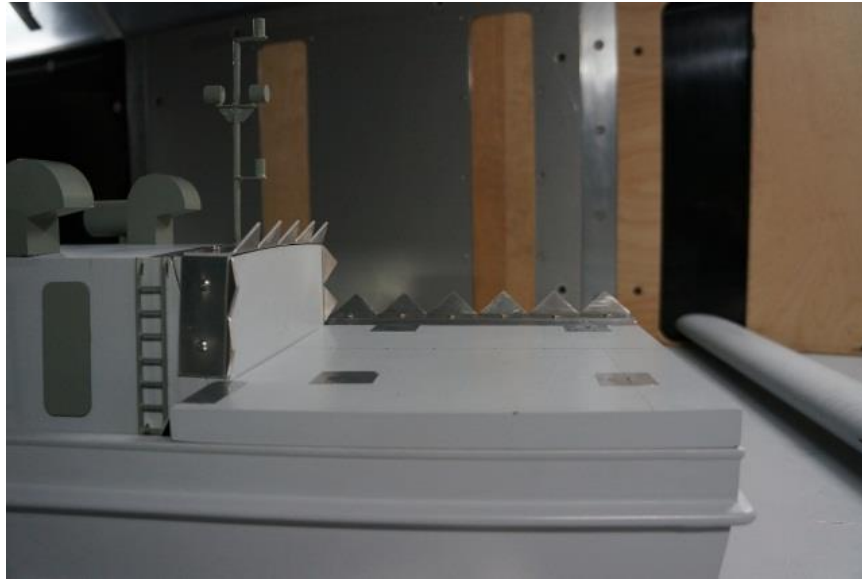
Figure 7. YP model with flow control fences

For this experiment a boundary layer splitter plate was installed in the tunnel 11 inches above the test section floor. The splitter plate was 101 inches long with a 2:1 elliptic leading edge and an approximate 3:1 half elliptic trailing edge profile. The splitter plate without the YP model installed creates a 13.33% solid blockage in the test section. Total blockage increases to 17.39% for the YP model with a 15° yaw angle.

2.3.1 Reference Coordinate System

A local ship coordinate system was established to plot the ship air wake. The $x = 0$ plane was set at the vertical hangar face; the $y = 0$ plane was set as the centerline of the ship; and the $z = 0$ plane was set as the flight deck surface. The x axis runs longitudinally along the ship with aft as the positive direction, the y axis laterally as starboard positive, and the z axis vertical with

distance above the flight deck as the positive direction. All data sampling locations and air wake

characteristic plots use this coordinate system as shown in Figure 8.
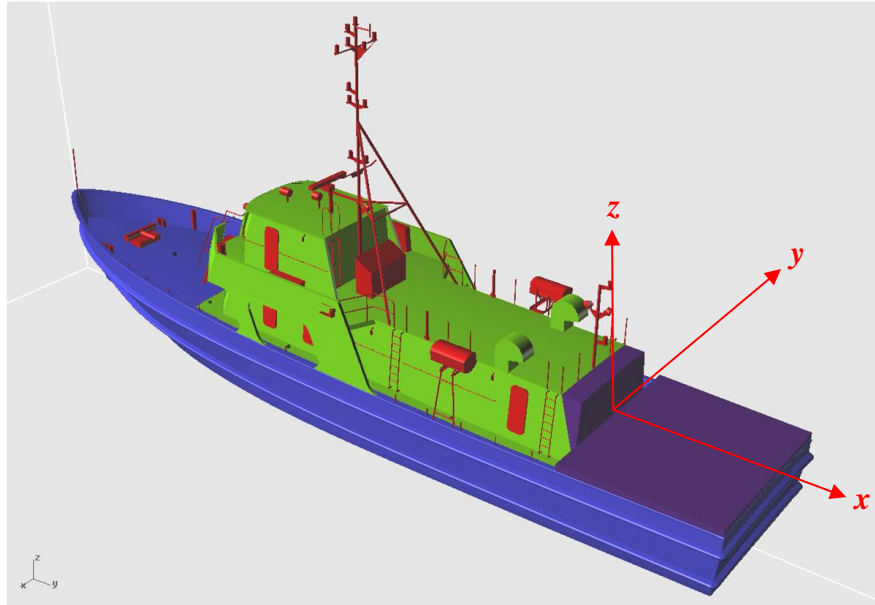
Figure 8. YP coordinate system

2.3.2 Instrumentation

This experiment used the Wake Interactive Survey Probe (WISP) system to survey the

ship air wake. The WISP system allows a flow probe to be moved through the air wake

according to a pre-determined grid pattern. For this investigation, WISP interfaced with an

Aeroprobe 12 hole Omniprobe to capture pressure measurements throughout the air wake. The

probe has a ¼ inch spherical tip containing 12 pressure taps distributed across its surface. Flow

velocity and direction are reduced from the pressure distribution over the surface of this sphere.

The Omniprobe is capable of accurately measuring flow angles up to ±150 degrees from the

forward end of the probe. This wide envelope allows the instrument to measure three

dimensional velocity components (u, v, w) free from bias errors and is able to identify reverse

flow without ambiguity. Flow measurements were taken with respect to the ship coordinate system where the nose of the probe was aligned with the x-axis. Figure 9 shows the Omniprobe mounted on a strut with the YP model installed in the tunnel.
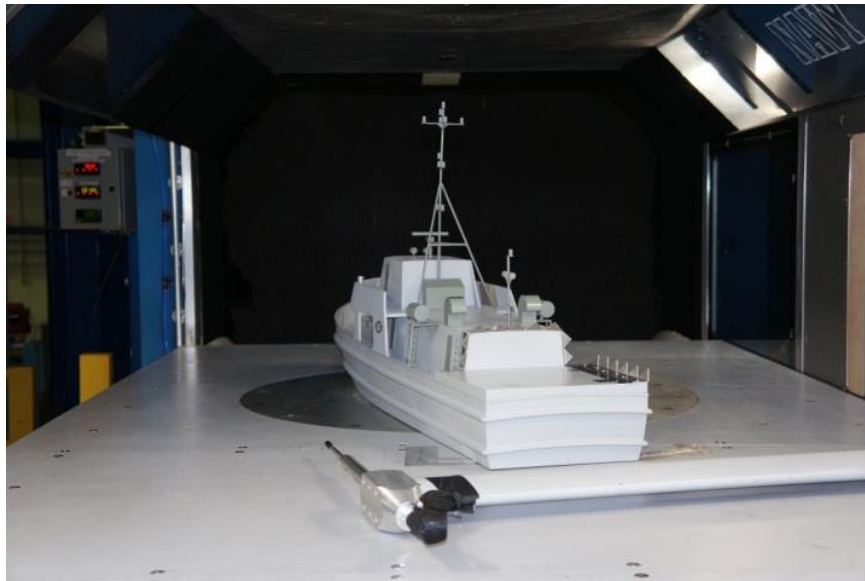
Figure 9. 12 hole Omniprobe and YP model in CCWT

Pressure readings were collected using the Pressure Systems Inc. System 8400 multichannel pressure scanning system. A 1 psi (lbf/in^2) gage electronically scanned pressure (ESP) module was connected to the Omniprobe pressure taps. 50 inches of pressure tubing connected the Omniprobe to the ESP unit.

Air wake scans were performed by an *yz*-traverse system consisting of two Newport IMS600 linear stages that created *y*- and *z*- motion respectively. Both stages have on-axis accuracies of 15 μm and have a maximum speed of 100 mm/sec. The traverse system was controlled by an XPS motion controller that communicated with the WISP system via an Ethernet connection. The WISP system created MATLAB based graphical user interfaces to provide for automated testing over a user defined test region.

2.3.3 Procedure

Air wake surveys of the 4% scale YP model were performed on six measurement planes perpendicular to the *x*-axis at distances of *x*/H = 0.452, 1.016, 1.504, 2.069, 2.558, and 3.122. Lateral constraints were -2.542 ≤ *y*/H ≤ 2.331 and 0.424 ≤ *z*/H ≤ 2.542. These limits were based on *in situ* test locations and safe operating margins for the probe to avoid contact with the fences on the starboard side of the flight deck and the horizontal flight deck surface. The same measurement planes were used for β = 0° and β = 15° testing. Figure 10 shows the YP model with the survey planes over the flight deck.
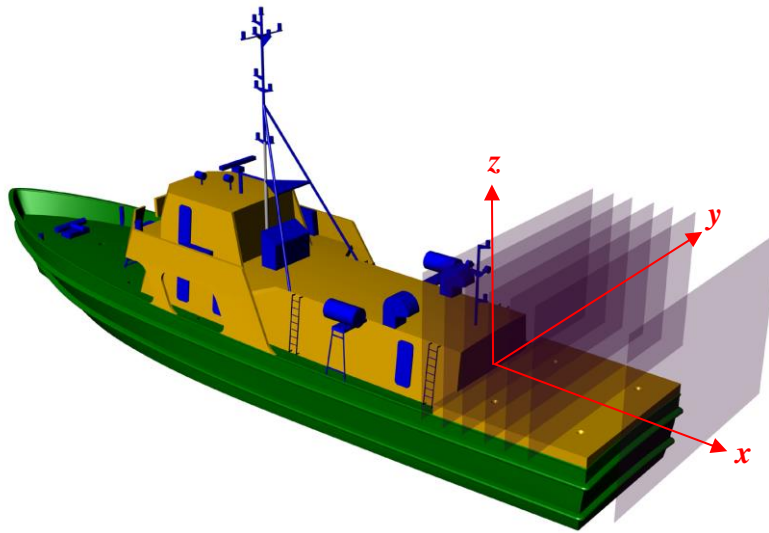
Figure 10. YP model and survey planes

A total of 253 data points were recorded for each survey plane (or 1518 total points for the entire air wake scan). The probe traversed each plane with a spacing of Δ*y*/H = Δ*z*/H = 0.212. The manufacturer recommended that the probe must be kept at least three diameters from solid surfaces to maintain data accuracy. Given a sphere diameter of ¼ inch, the minimum

coordinates were $[x/H]_{min} = [z/H]_{min} = 0.32$.   This recommendation was met using the test regions defined above.

The Reynolds number based on the length of the model was maintained at 7.412 x 10^6 ± 0.100 x 10^6. Testing was conducted with tunnel velocities of 289.0 ± 5.8 feet per second. The data sampling rate was based on acquiring 60 measurement sets at 1 ms delay between sets with each set containing 40 data frames at 100 μs delay between frames. The gross sampling rate was 340 Hz over 7.1 sec. Prior to data sampling, the flow was allowed to stabilize for approximately 7 seconds after probe movement.

Each plane was sampled with the probe in an upright then inverted orientation in order to determine and remove any position bias error. By negating the inverted probes flow pitch and yaw angles determined from equations (1) and (2), the two measurements were effectively averaged. Local probe errors, δ_α and δ_β, were determined using equations (3) and (4). Summing these values effectively differenced the two magnitudes. The bias errors ranged from -0.15 to 0.02 deg for α and -0.71and 0.58 deg for β. The estimated uncertainty in pitch and yaw angle measurements after bias corrections was determined as the standard deviations in δ_α to be 0.06 deg and in δ_β to be 0.47 deg.

$$\alpha_{corr} = \frac{1}{2}\left(\alpha_{upright} - \alpha_{inverted}\right) \qquad (1)$$

$$\beta_{corr} = \frac{1}{2}\left(\beta_{upright} - \beta_{inverted}\right) \qquad (2)$$

$$\delta_\alpha = \frac{1}{2}\left(\alpha_{upright} + \alpha_{inverted}\right) \qquad (3)$$

$$\delta_\beta = \frac{1}{2}\left(\beta_{upright} + \beta_{inverted}\right) \qquad (4)$$

The wind tunnel testing in this investigation was performed with very close adherence to the instrumentation, procedures, and analysis methods used in previous USNA Ship Air Wake wind tunnel research as performed by Miklosovic, Kang, and Snyder [17]. The only difference in instrumentation between the no fence wind tunnel experiments and the testing conducted for this investigation was the Aeroprobe Omniprobe. Previous testing without the fences installed on the YP model used an older model 18-hole Aeroprobe Omniprobe with a 3/8 inch brass sphere tip. The original 18-hole Omniprobe was not available for this experiment. Consequently, a newer 12-hole Omniprobe was used with a ¼ inch sphere tip. The 12-hole and 18-hole instrument use the same method to measure mean velocity.

A test was performed with the 12-hole Omniprobe to confirm it was satisfactory to use in comparisons with the older 18-hole instrument. Ten points were sampled within the air wake for the original YP model without flow control fences. Six of the test locations showed good agreement in both direction and magnitude. The other four locations showed error in flow direction when the Omniprobe was close to the surfaces of the YP model. The rest of the wind tunnel instrumentation was double checked to ensure there were no other setup issues and that the Omniprobe was the main source of the measurement differences. No issues with the setup were found, so the 12-hole Omniprobe was used for testing, noting the results from the short comparison test. Each data run was checked to ensure the measured flow direction followed expected ship air wake theory. Any erroneous data points that were in clear violation of the physics of a ship air wake (e.g. flow in or out of a surface) were omitted.

3   Beta 0 Results

Analyzing a ship air wake flow field is a difficult problem that requires the use of multiple data collection and analysis tools to fully realize the flow field and its structures. Numerical simulations and wind tunnel experiments can be useful tools for aerodynamic studies, but the limitations of these two experimental methods must be discussed before the results can be used individually to assess changes induced in an air wake. This paper will first compare CFD and wind tunnel results with *in situ* measurements to discuss limitations and applicability of the two experimental techniques. This paper will then evaluate the effects of the flow control fences using *in situ* measurements, numerical simulations, and wind tunnel experiments. Test metrics will be described prior to application.

3.1   CFD Validation

Numerical simulations were run on the YP model without flow control fences with a uniform boundary layer input at 7 knots relative wind speed over deck and standard atmosphere temperature and pressure. Discussion of CFD validation will focus on the YP air wake without flow control fences. The Reynolds number for the simulations was 8.1256×10^6 based on the length of the YP. Figure 11 shows *in situ* and CFD air wake data for the YP in a headwind. The figure shows a normalized velocity data on a longitudinal plane along the ship's centerline, looking at the port aspect. A vector of length one is plotted for reference of the normalized velocity. The hangar and flight deck outline are also plotted to show relative size of the ship and

the air wake. The *x*/H axis runs fore and aft along the ship with aft as the positive direction, and the *z*/H axis is vertical with distance above the flight deck as the positive direction.
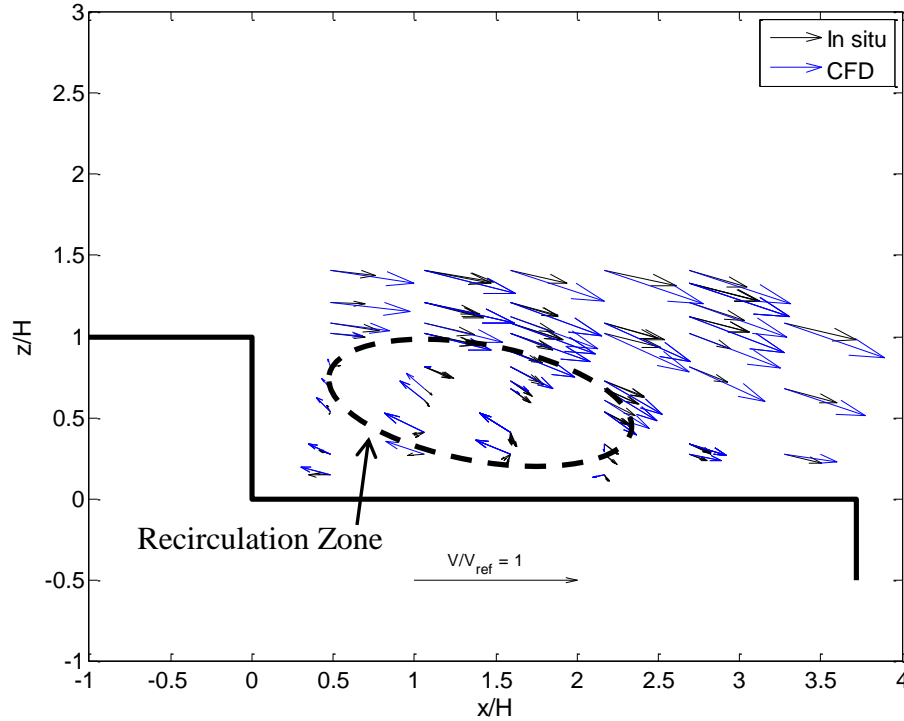
Figure 11. *In situ* vs. CFD at *y*/H = 0 for β = 0° with 7 kt uniform CFD inflow

Qualitatively the CFD and *in situ* results have a good directional agreement above the recirculation zone. However, CFD predicted higher velocity magnitudes at each test location throughout the air wake. Within the recirculation zone CFD shows a more dramatic reverse flow section whose center is farther aft along the flight deck. The CFD shows the reattachment point at *x*/H = 2.5, while the *in situ* measurements places the reattachment point at *x*/H = 2.

The mean streamwise velocity ($<u>$) profile at a centerline location can be used to quantify the ship air wake. The mean streamwise velocity component is important because Bramwell [18] has shown that reducing the horizontal velocity component through a helicopter

disk rotor will reduce thrust. This response is particularly noticeable at the forward speeds a

helicopter would be traveling relative to the air wake during a shipboard launch or recovery

operation. In addition, the mean velocity gradient is important to understanding the second order

nature of a flow. This investigation used the mean streamwise velocity profile at x/H = 1.59 and

y/H = 0 because this point represents the approximate center of the flight deck and a possible

location for a helicopter to touch down.

Figure 12 compares the mean streamwise velocity profile for the *in situ* and CFD results

without flow control fences at x/H = 1.59 and y/H = 0. The individual *in situ* measurements are

plotted, and a line is drawn to represent the average normalized streamwise velocity at each test

height. The plot shows that the CFD simulations predict a higher mean streamwise velocity

gradient (d<u>/dz), which corresponds to higher turbulent kinetic energy production in the flow.

In addition, CFD predicts higher absolute velocity magnitudes for heights below z/H = 0.4 and

above z/H = 0.65. At hangar height (z/H = 1), CFD predicts a mean streamwise velocity that is

51.4% larger than the *in situ* results.
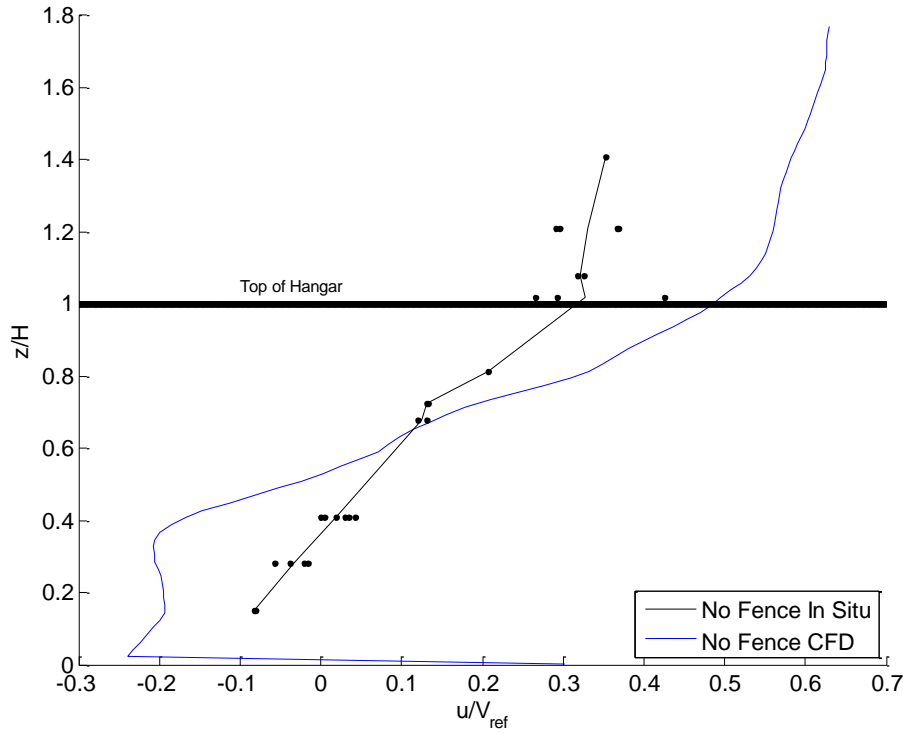
Figure 12. Mean *u* velocity profile at *x*/H = 1.59, *y*/H = 0 for β = 0° with 7 kt uniform CFD inflow

The u_{rms} velocities in the air wake at individual test locations can be used to describe the velocity fluctuation level within the flow. Velocity fluctuations in an air wake are important to quantify because changes in velocity may result in increased pilot workload during launch and recovery operations. Figure 13 shows the velocity standard deviation profile for the YP air wake at *x*/H = 1.59 and *y*/H = 0. Numerical simulations predict higher standard deviation values than *in situ* testing for heights less than *z*/H = 1.21. CFD shows a higher peak velocity standard deviation of 0.19 at *z*/H = 0.876, while *in situ* has a maximum standard deviation of 0.08 at this height. At the height of the hanger, CFD predicted velocity fluctuation levels that are 34.8% higher than the *in situ* results. Overall, *in situ* measurements show a more uniform velocity

fluctuation level distribution with respect to height than the CFD predictions. Larger CFD

velocity fluctuation levels correspond to the greater CFD streamwise velocity gradient discussed

above.
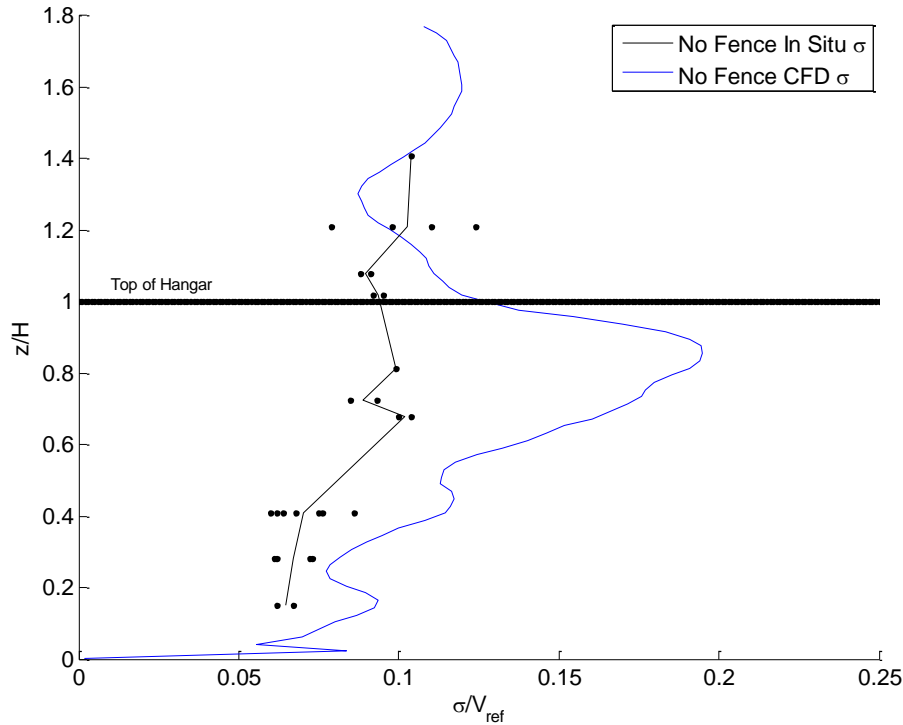
Figure 13. Velocity standard deviation at x/H = 1.59, y/H = 0 for β = 0°

The differences shown by the centerline mean velocity profile, mean streamwise velocity

gradient, and u_{rms} profile for the CFD and *in situ* results suggest that the numerical simulations

used for this investigation do not provide a highly accurate model of the YP's air wake. CFD

can be used as a rough estimate of the air wake and can be applied to the study of passive flow

control to provide an initial understanding of how a passive flow control device might change the

air wake, but validation with i*n situ* measurements is needed before final conclusions can be

made.

The differences between *in situ* measurements and the CFD simulations discussed above can be attributed to two factors: the presence of an atmospheric boundary layer during underway testing and the dynamic nature of *in situ* measurements. The CFD simulations used in the discussion above do not account for the atmospheric boundary layer profile that exists on the surface of the Chesapeake Bay during underway testing. An atmospheric boundary layer creates a different streamwise velocity profile, which could contribute to the differences between the CFD and *in situ* velocity gradients seen at the center of the flight deck. The turbulence in the air wake inflow for *in situ* measurements was not properly modeled by these simulations; therefore significant differences can be seen between the CFD and *in situ* mean velocity predictions. Second, underway testing is subject to constantly changing winds that the helmsman must correct for to stay within the acceptable ±5 degree Beta range. The yaw movements required to maintain the desired Beta test condition may induce additional velocity components into the flow that cause changes to the recirculation zone and shear layer not present in CFD simulations where the YP maintains a more controlled, constant yaw angle relative to the incoming flow.

3.2 Wind Tunnel Validation

Wind tunnel testing was performed at a Reynolds number of 8.1256×10^6 based on the length of the YP model. This test corresponds to *in situ* results collected at 7 knots relative wind over deck. The wind tunnel scan area did not sample the exact locations used for underway testing so the wind tunnel results were interpolated to match *in situ* sampling locations. Due to the limitation of Omniprobe accuracy at distances of less than 3 diameters from a solid surface,

the minimum height for wind tunnel results was limited to $z/H = 0.3178$ so it was more difficult

to capture the reattachment point with wind tunnel testing than *in situ* measurements.

A comparison between wind tunnel and *in situ* measurements will help show the

applicability of using wind tunnel data to model full scale testing. Discussion in this section uses

the data collected without the flow control fences installed. Figure 14 presents the mean velocity

profiles of the air wake for the centerline of the YP in a headwind condition. The plot shows that

that the wind tunnel and *in situ* testing have good qualitative velocity vector agreement in both

magnitude and direction above the recirculation zone. The center of the recirculation zone also

matches for the two data sets.
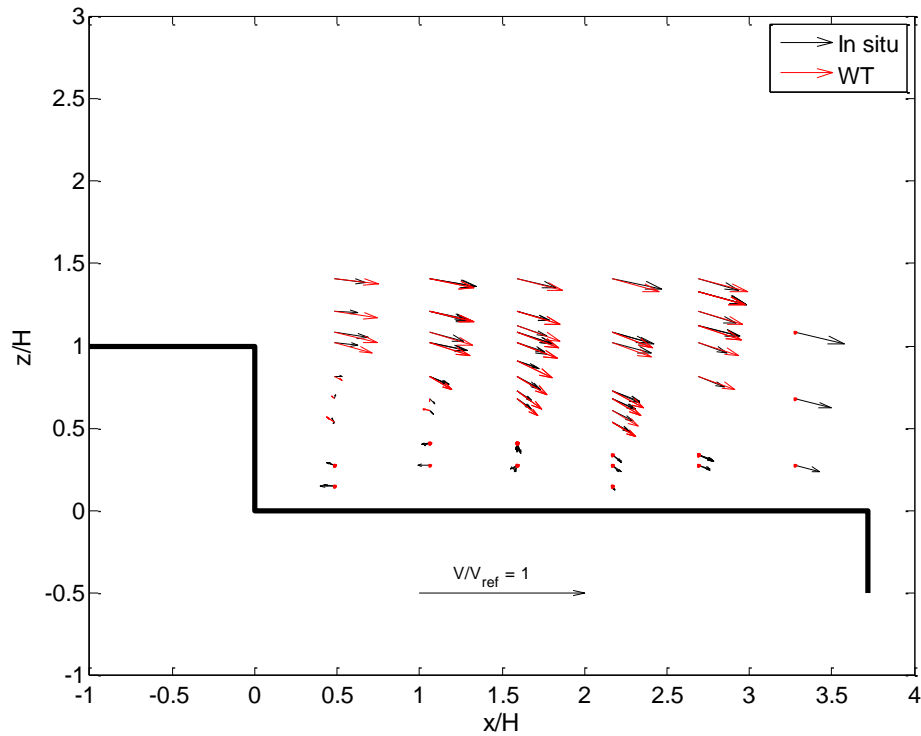
Figure 14. *In situ* vs. wind tunnel at $y/H = 0$ for $\beta = 0°$

Further analysis of the wind tunnel and *in situ* results can be made using mean

streamwise velocity profile at $x/H = 1.59$ and $y/H = 0$. Figure 15 shows the mean streamwise

velocity profile comparison between wind tunnel and *in situ* measurements for the no fence

configuration at $\beta = 0°$. The wind tunnel experiments measured a larger streamwise velocity

gradient below $z/H = 1$. Above the hangar, *in situ* and wind tunnel results have a similar velocity

gradient but the wind tunnel results have a normalized mean streamwise velocity component that

is 28.66% higher than the *in situ* data.
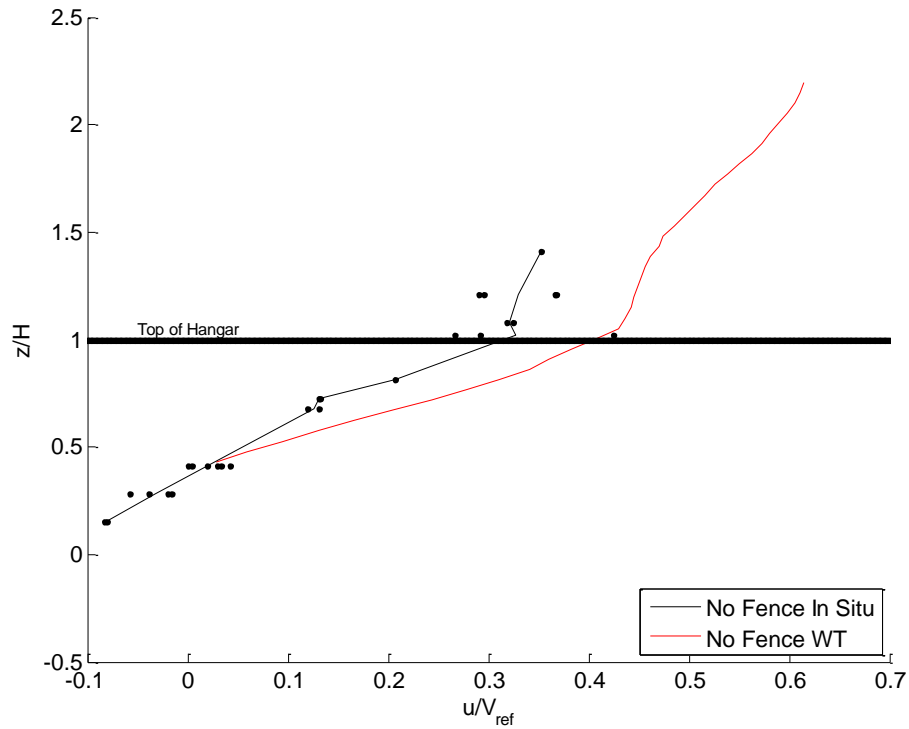
Figure 15. Mean streamwise velocity profile at $x/H = 1.59$, $y/H = 0$ for $\beta = 0°$

The stronger shear measured in the wind tunnel can be attributed to the atmospheric

boundary present for underway testing. The wind tunnel setup used for this investigation does

not have an induced atmospheric boundary layer profile to model the underway testing

environment. This difference in inflow manifests itself in different mean velocity gradient measured at the center of the flight deck. Wind tunnel experiments can be used to model full scale underway testing, but caution must be used when making a direct comparison to the *in situ* environment. Larger wind tunnel velocity gradients may provide misleading results when trying to quantify the effects the air wake may have on a helicopter. Wind tunnel testing can be confidently applied to the study of passive flow control, but final conclusions need to be validated by *in situ* measurements.

3.3   Flow Control Fence Analysis: Mean Velocity

3.3.1 In situ

Underway measurements can be analyzed by looking at the centerline plane of the ship for the headwind condition. Figure 16 presents a quiver plot of the *in situ* measurements for both ship configurations. The plot shows the enlargement of the recirculation zone and the aft movement of the reattachment point. The no fence data places the reattachment point at $1.5 < x/\text{H} < 2$, while the flow fences move the reattachment location aft to $2 < x/\text{H} < 3$. This aft movement corresponds to the increased effective hangar height with the addition of the fences. The fences also caused the recirculation zone to grow vertically, moving the shear layer above the height of hangar.
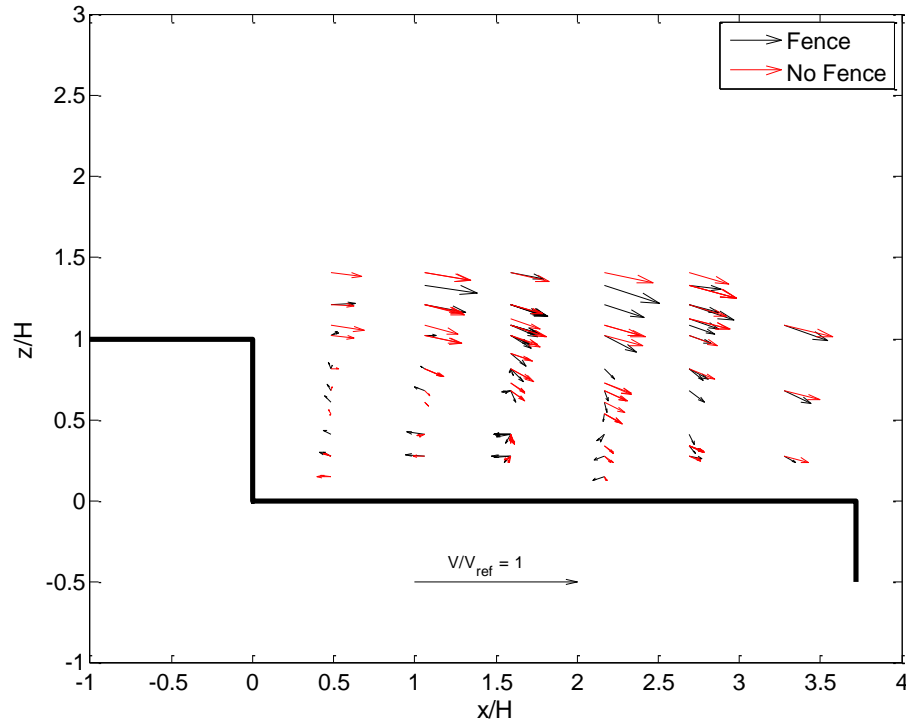
Figure 16. I*n situ* data at y/H = 0 for $\beta = 0°$

The mean streamwise velocity profile for both configurations can show the change the

fences cause on the velocity gradients of the air wake. Figure 17 presents the mean streamwise

velocity profile of the air wake at x/H = 1.59 and y/H = 0. All of the sampled data is plotted as

individual points, and the average lines are overlaid. The plot shows that the fences do not cause

a significant change in the streamwise velocity gradient for z/H < 1. However, the fences

produce more shear above the hangar height, which corresponds to the vertical movement of the

shear layer shown above.
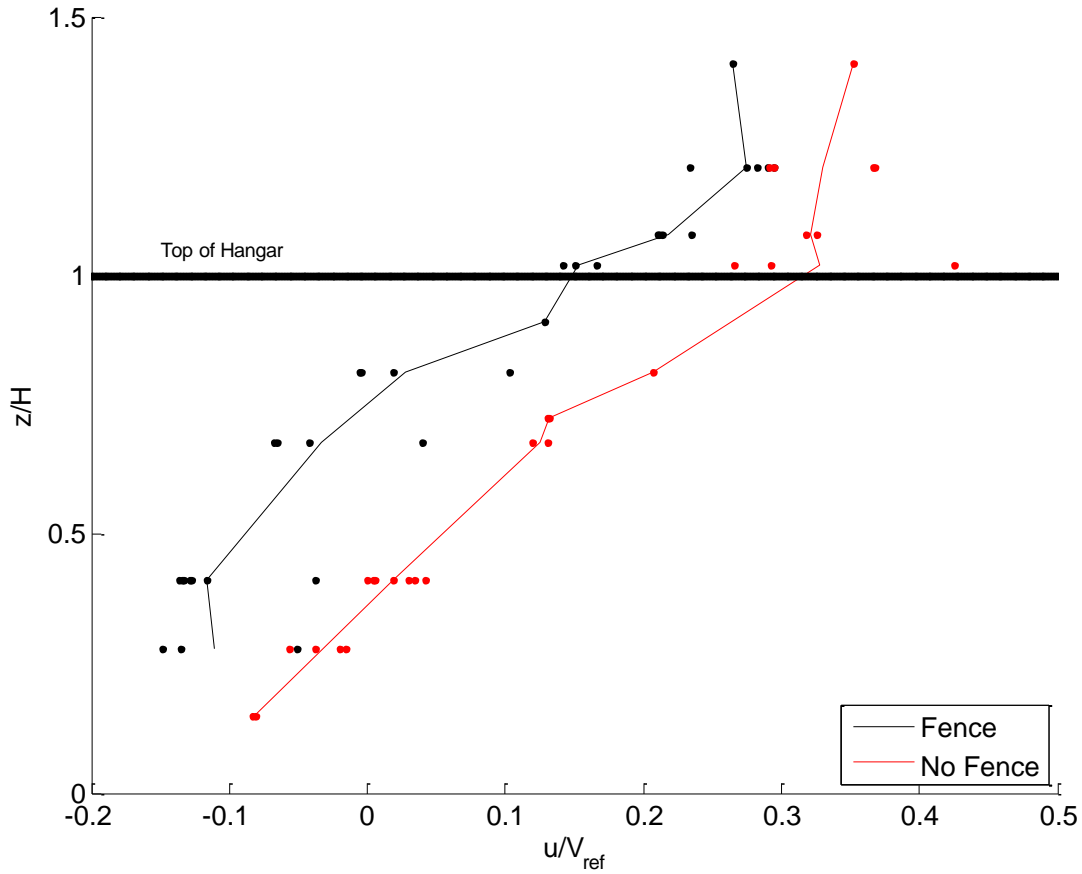
Figure 17. Mean streamwise velocity profile at x/H = 1.59, y/H = 0 for β = 0°

Figure 18 shows the streamwise u_{rms} velocities for the *in situ* results at x/H = 1.59 and y/H = 0. At z/H = 1, the fences cause a 7.4% increase in velocity standard deviation. The fences have a maximum streamwise velocity fluctuation of 0.117 at z/H = 1.08, while the no fence configuration produces a maximum value of 0.102 at z/H = 0.678. The fences produce higher streamwise velocity fluctuation levels above hangar height (z/H = 1). This result corresponds to the increase in shear above the hangar height discussed above.
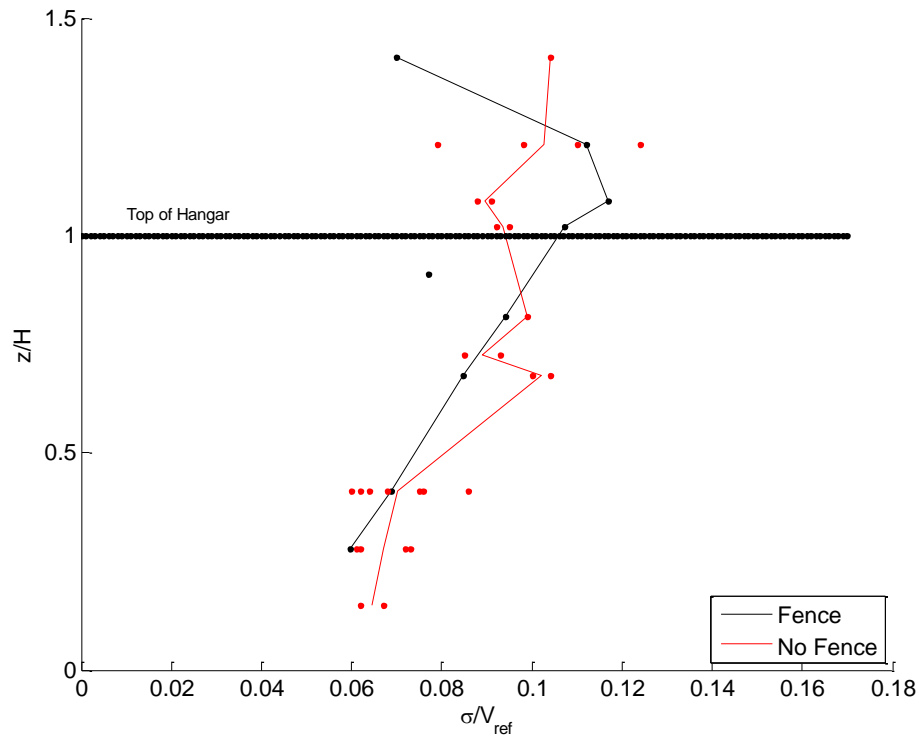
Figure 18. Velocity standard deviation at *x*/H = 1.59, *y*/H = 0 for β = 0°

3.3.2 Computational Fluid Dynamics

CFD can be a powerful tool for analyzing the effects of the flow control fences because of the large number of possible sampling locations. Given the differences between CFD and *in situ* results discussed above, a comparison can be made between the fence and no fence configuration using CFD simulations, but some caution must be taken directly applying the quantitative results to full scale YP testing.

CFD analysis of the flow control fences uses simulations with a 20 kt uniform boundary layer inflow for a headwind condition. Simulations were run with a Reynolds number of 23.216 x 10^6 based on the length of the YP and standard temperature and pressure.

Figure 19 shows CFD predictions along the centerline plane of the YP for the fence and no fence configurations. This figure shows how the fences create a larger recirculation zone and move the reattachment point moves aft along the flight deck from approximately $x/H = 2$ to $x/H = 3$.
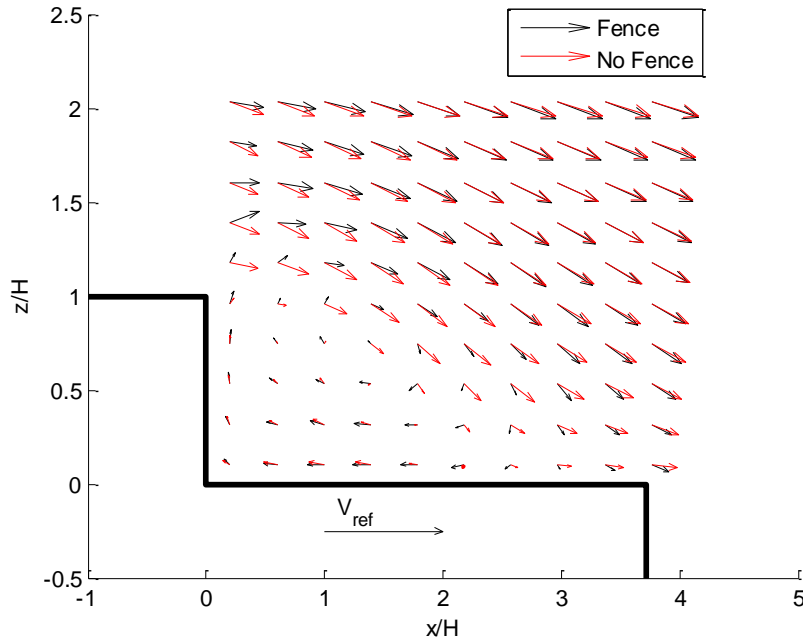
Figure 19. CFD data at $y/H = 0$ for $\beta = 0°$

The mean streamwise velocity profile at $x/H = 1.59$ and $y/H = 0$ is shown in Figure 20 for the fence and no fence configurations. The figure shows that the fences do not change the velocity gradient below hangar height, but there is more shear above $z/H = 1$. The two flow fields converge at $z/H = 1.73$, and CFD predicts the fences will no longer have an effect on the streamwise velocity gradient of the air wake at the center of the flight deck ($x/H = 1.59$, $y/H = 0$). The fences also create a 25% loss in streamwise velocity at hangar height.
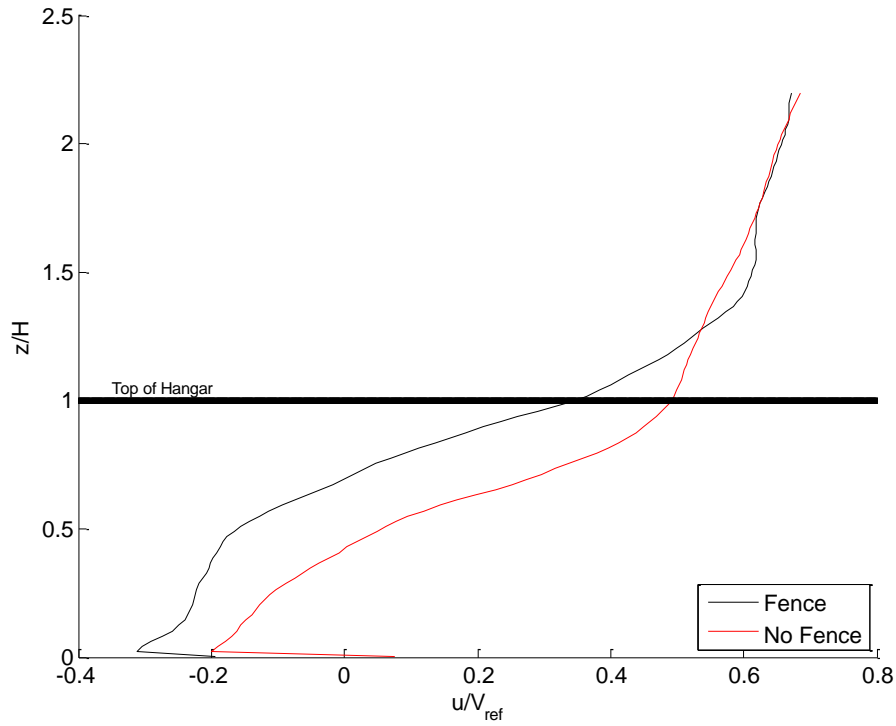
Figure 20. Mean streamwise velocity profile at $x/H = 1.59$, $y/H = 0$ for $\beta = 0°$

Figure 21 presents the streamwise u_{rms} velocities at $x/H = 1.59$ and $y/H = 0$. This plot show that the fences move the vertical location of maximum velocity fluctuation level from $z/H = 0.55$ to $z/H = 0.84$. This vertical movement is due to the increase in effective hangar height and the enlargement of the recirculation zone, which causes more shear to develop at hangar height. At $z/H = 1$, the fences cause a 50% increase in the velocity fluctuation level.
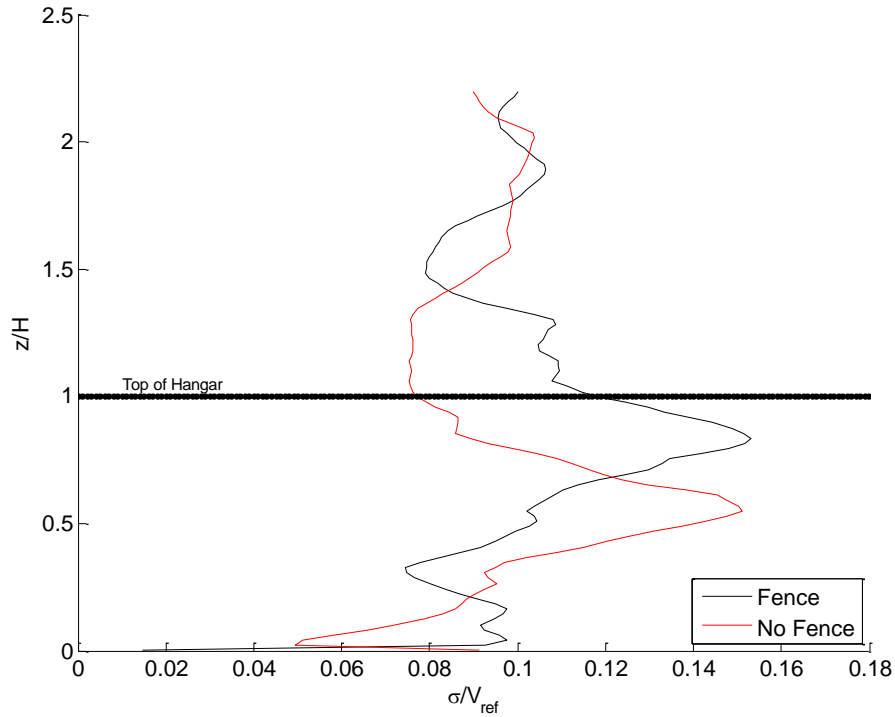
Figure 21. Velocity standard deviation at $x/H = 1.59$, $y/H = 0$ for $\beta = 0°$

3.3.2.1 Disk Rotor Analysis

Bramwell shows that downwash can have an impact on rotor thrust such that increasing downwash will reduce thrust produced by a helicopter [18]. Therefore it is important to quantify the downwash through a helicopter rotor area to discuss changes in a ship air wake. The SH-60S was chosen as the representative helicopter for this analysis because it will be one of the primary aircraft in future fleet operations. The main rotor area for SH-60S was scaled to YP 676 based on the flight deck area of DDG 79, a Flight IIA Arleigh Burke Class Destroyer. Mean velocity and standard deviation data were collected over a grid of points within the helicopter rotor area. Four unique rotor locations were created: On Deck, Low Hover, High Hover, and High Hover crossing the Aft end of the flight deck. The On Deck position represents the height of a SH-60S

while sitting on the flight deck. This height was scaled to the YP based on the hangar height of

DDG 79. Low Hover represents the helicopter at one fourth of a rotor diameter above the flight

deck surface. High Hover was set at half a rotor diameter above the flight deck. For these three

test heights, the center of the rotor was placed at the center of the YP flight deck, x/H = 1.89 and

y/H = 0. The High Hover Aft position used the same height as the High Hover location (0.5x

rotor diameter above the flight deck) but moved the rotor center position along the centerline to

the aft end of the flight deck (x/H = 3.77 and y/H = 0). These heights represent areas where

pilots would possibly be affected by the ship air wake as they make their final approach for a

shipboard landing. Figure 22 shows the four test locations and the size of the SH-60S scaled

rotor diameter relative to the YP model. Each rotor disk area is comprised of 901 points.
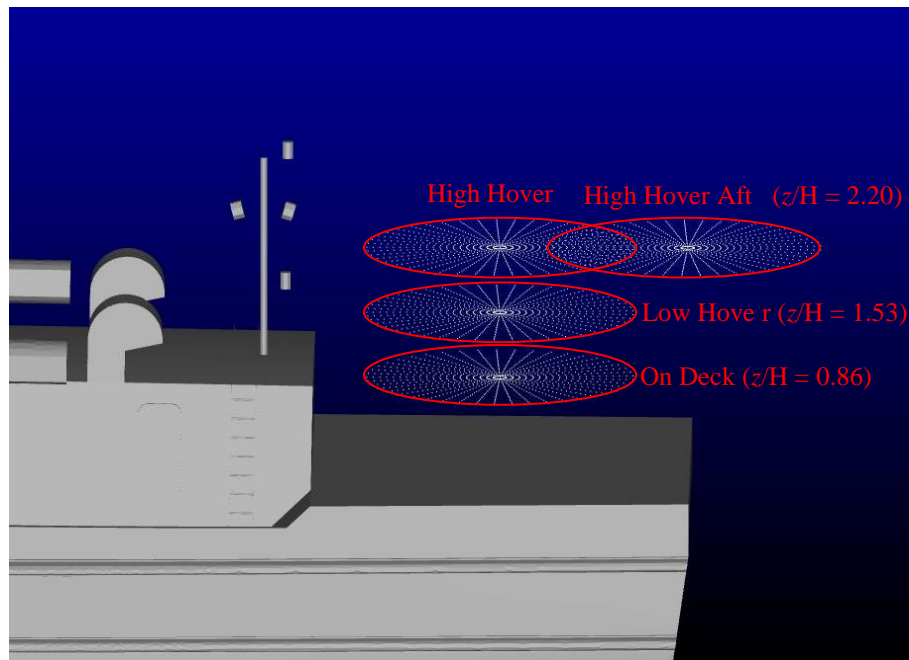
Figure 22. Disk rotor test locations

The disk rotor downwash method was applied to CFD simulations run with a 20 knot uniform boundary layer inflow at zero yaw. Table 1 shows the average downwash velocity w and the w_{rms} velocity across the rotor. The fences created a lower average downwash velocity through the disk rotor for the on deck and low hover positions, caused no significant change for the high hover position, and produced higher downwash velocities at the aft high hover location. The decrease in downwash at the on deck and low hover positions corresponds to the growth of the recirculation zone and the aft movement of the reattachment point. Downwash was nearly unaffected at the high hover position, showing that the fences may not cause any significant changes in helicopter rotor thrust above a height of $z/H = 2.20$. The aft hover position experienced a larger downwash, which is most likely due to the enlargement of the recirculation zone and the aft movement of the reattachment point.

Using standard deviation as the metric for the velocity fluctuation level within the rotor area, velocity standard deviation increased for the on deck, high hover, and high hover aft positions. The on deck position saw the largest increase in velocity fluctuations of 16%, while the low hover position experienced a 2% decrease. Increased flow velocity fluctuation levels across the rotor area could translate to higher pilot workload.

Table 1. Disk Rotor downwash velocity (w) and w_{rms} for CFD simulations

Position	Fence		No Fence	
	w (ft/s)	w_{rms}	w (ft/s)	w_{rms}
On Deck	-3.1692	3.3428	-4.6975	2.8828
Low Hover	-4.7513	2.7885	-4.8461	2.8441
High Hover	-2.8436	2.9673	-2.8534	2.6352
Aft Hover	-3.1496	2.4272	-2.7857	2.1286

Overall, a CFD based analysis of the fences shows that this passive flow control device creates a lower velocity region at the center of the flight deck, while increasing velocity fluctuation levels at the hangar height and moving the location of peak fluctuation upwards. Disk rotor analysis shows lower downwash velocities at the lower flight positions and increased velocity fluctuation levels. The CFD simulations show that fences may have an impact on rotor thrust through changes in the mean u and w velocity components, and handling capabilities with the increase in velocity standard deviations at the lower flight positions.

3.3.3 Wind Tunnel

Discussion of the effectiveness of the flow control fences can be expanded using the wind tunnel test results. Figure 23 shows the wind tunnel mean velocity measurements along the centerline plane for the fence and no fence configurations. The plot shows good agreement in flow direction and velocity magnitude above the recirculation zone. However, the flow measurements with the flow control fences installed do not clearly show the recirculation zone or a significant region of reversed flow. This data was acquired with the new 12-hole Omniprobe. The rest of the equipment used in the wind tunnel instrumentation worked properly in initial tests. The newer probe may have had trouble measuring the turbulent flow found within recirculation zone due to fewer pressure taps and a smaller tip diameter compared to the older 18-hole design. No definite conclusions can be drawn about the functionality of the Omniprobe from the experiments conducted in this investigation, but the data outside the recirculation zone can be confidently used for ship air wake analysis. Future discussion using the wind tunnel data

will ignore data from within the recirculation zone that clearly disagrees with accepted ship air

wake flow physics.
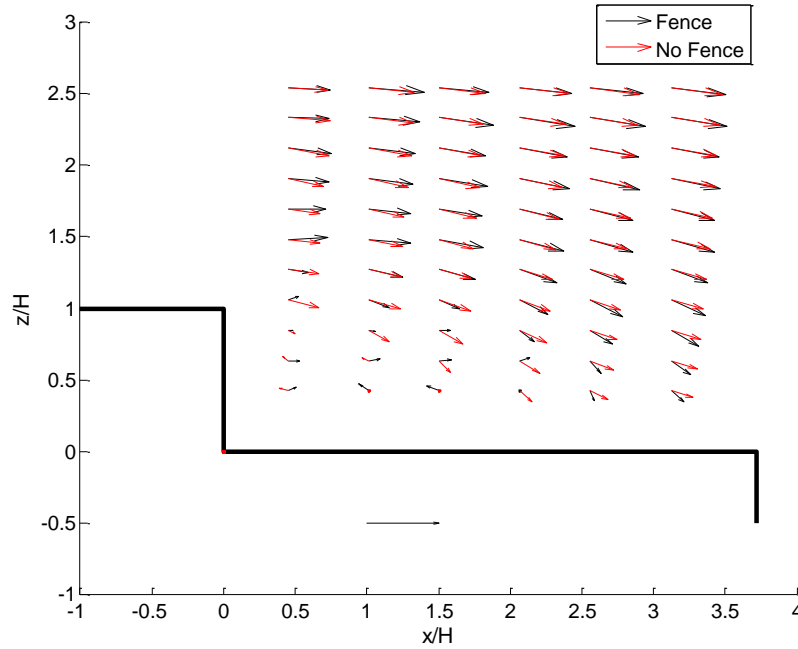
Figure 23. Wind tunnel data at $y/H = 0$ for $\beta = 0°$

Figure 24 presents the mean streamwise velocity profile at $x/H = 1.59$ and $y/H = 0$. Data

for the fence configuration below $z/H = 1$ has been included but should be discussed with caution

based on the data errors discussed above (strange measurements within the recirculation zone

with the new Omniprobe). Figure 24 shows that the fence and no fence configurations produce

the same amount of shear below hangar height. For the region $1 < z/H < 1.4$, the fences create a

larger streamwise velocity gradient. This result coincides with the increase in shear seen by *in

situ* measurements and numerical simulations.
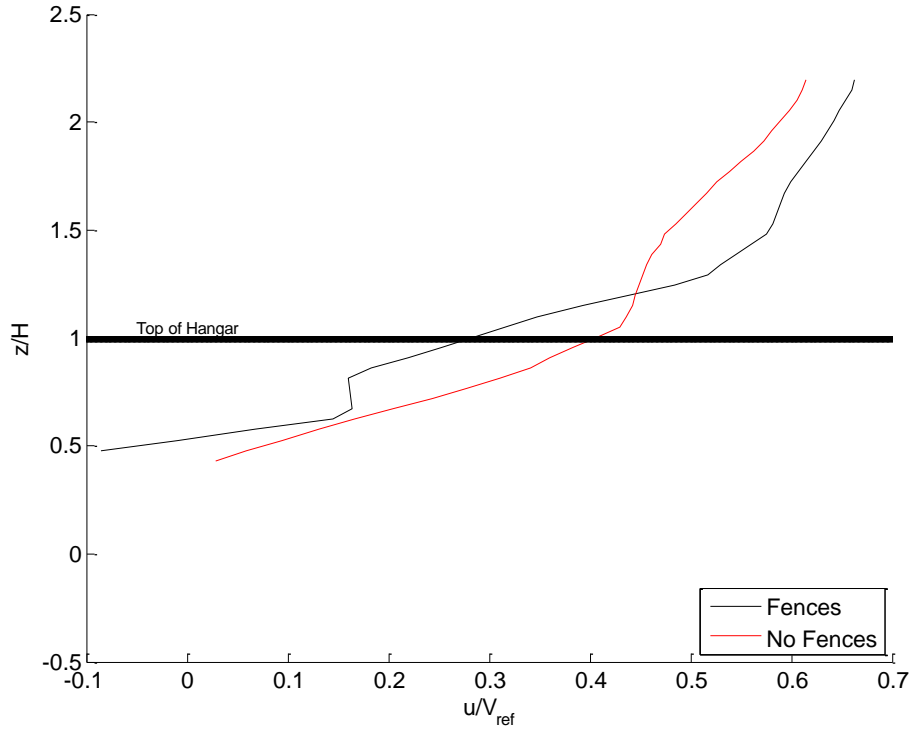
Figure 24. Mean *u* velocity profile at *x*/H = 1.59, *y*/H = 0 for β = 0°

3.3.3.1 Vorticity

Air wake vorticity, a measure of the rotational component of velocity, is another metric

for quantifying the changes to the ship air wake due to the flow control fences. The non-

dimensional axial component of vorticity can be calculated using equation (5)

$$\widetilde{\omega}_x = \frac{\omega_x H}{V_\infty}$$

(5)

where ω is vorticity, H is the hangar height of the scale YP model (2.361 inches), and V_∞ is the

free stream velocity of the wind tunnel. Figure 25 shows the surface plots of the air wake

vorticity for the fence and no fence configurations at zero yaw for the plane *x*/H = 1.504. *v* and

w velocity component vectors are plotted for each sampling location and vorticity is colored by

strength. The individual flow vectors at each test location show that the fence data set has some

abnormal flow characteristics near the flight deck. Plot a) shows vertical velocity components at $z/H = 0.5$, a result that disagrees with accepted air wake flow physics (*in situ* data shown above supports this claim). Abnormal vertical velocity components can be seen up to a height of $z/H = 0.85$. The source of these potential measurement errors is discussed above and more detailed analysis of the 12-hole Omniprobe is required to make definitive conclusions about the equipment. However, for the purposes of analyzing the effects of the flow control fences, the flow vorticity can be used to comment on the air wake above $z/H = 1$. Plots a) and b) show a similar vorticity profile above the top of the hangar with regions of high vorticity extending vertically from $z/H = 1$ to $z/H = 2$ at the corners of the hangar. Along the centerline of the ship, the fences generate higher vorticity above $z/H = 1$.
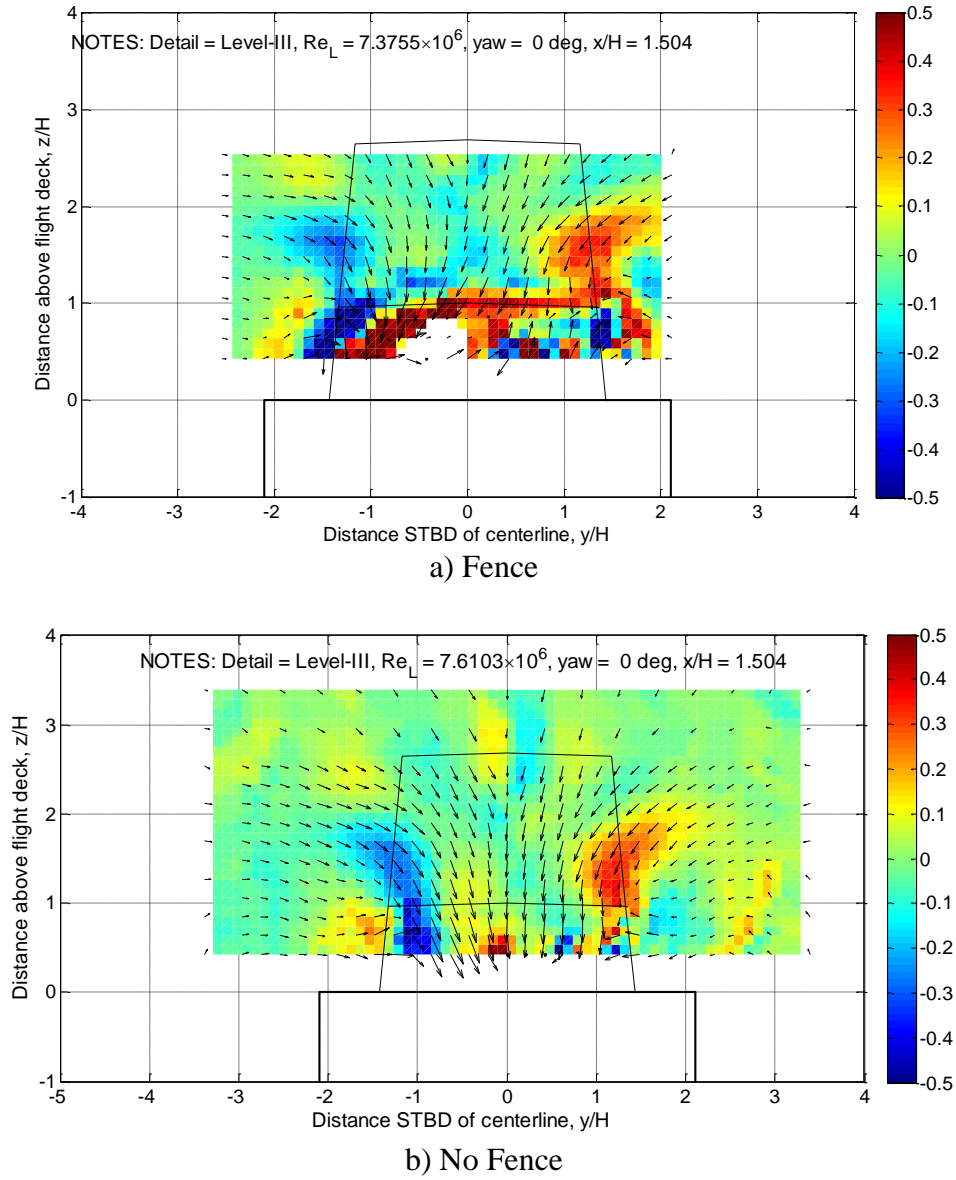
a) Fence

b) No Fence

Figure 25. Surface plots of wake vorticity for $\beta = 0°$ at $x/H = 1.504$: a) fence, b) no fence configuration

3.3.3.2 Disk Rotor Analysis

The disk rotor method can also be applied to the wind tunnel results. Due to the need to interpolate the wind tunnel data set to obtain downwash velocities for the points within the rotor disk cloud, only the On Deck, Low Hover, and High Hover positions can be analyzed. The Aft

High Hover position does not allow for an entire SH-60S rotor area to be placed inside the wind tunnel sampling area so results cannot be interpolated to cover the whole rotor area. The disk rotor method can be applied to the wind tunnel data given the Omniprobe concerns discussed above because there is sufficient agreement in the mean velocity vectors for the fence and no fence data sets above the shear layer (above z/H = 0.85). The On Deck position has a height of z/H = 0.86 so the data at this position can be used for analysis. The other flight positions are higher above the flight deck so they are also acceptable to use with the disk rotor method.

Table 2 presents the disk rotor downwash velocities for the wind tunnel testing. The wind tunnel predicts lower downwash velocities with fences for all three flight positions with a maximum difference of 26.3% for the On Deck position. This result matches the CFD disk rotor analysis that also showed a decrease in average downwash across the rotor for the On Deck and Low Hover flight positions. Wind tunnel testing suggests that, according to Bramwell's theory, the fences will increase rotor thrust by decreasing downwash.

Table 2. Disk Rotor downwash from wind tunnel experiments

Position	w Fence (ft/sec)	w No Fence (ft/sec)
On Deck	-1.3377	-1.8159
Low Hover	-1.4830	-1.5704
High Hover	-1.1501	-1.2810

3.4   Flow Control Fence Analysis: Turbulence Statistics

Time history data from *in situ* measurements can show the high level turbulent velocities that exist within a ship air wake. It is important to quantify the frequency of turbulence within

the ship air wake to determine if the fences create adverse effects beyond changes to the mean velocity profile of the flow. The overall flow structure can be visually identified by the recirculation zone and the reattachment point; however, the turbulence affecting helicopter stability can be quantified by the high order statistics of the velocity fluctuations. *In situ* time history data has been analyzed with energy spectra and weighted joint probability density functions.

3.4.1 Energy Spectrum

Energy spectra describe the energy density depending on the scales of fluid motion. Applying energy spectra to ship air wake analysis can show the length scale of eddies formed over the flight deck and whether or not the fences have a significant impact on turbulent energy dissipation. Energy spectra are defined by equation (6),

$$E(k, \varepsilon) = C\kappa^{-5/3}\varepsilon^{2/3} \tag{6}$$

where C is the Kolmogorov constant, κ is wave number and ε is the rate of energy dissipation per unit volume.

Figure 26 provides a sample schematic of the energy spectrum. An energy spectrum has a slope of -5/3 in the inertial range. Note that the wavenumber is inversely proportional to the scale of the fluid motion.
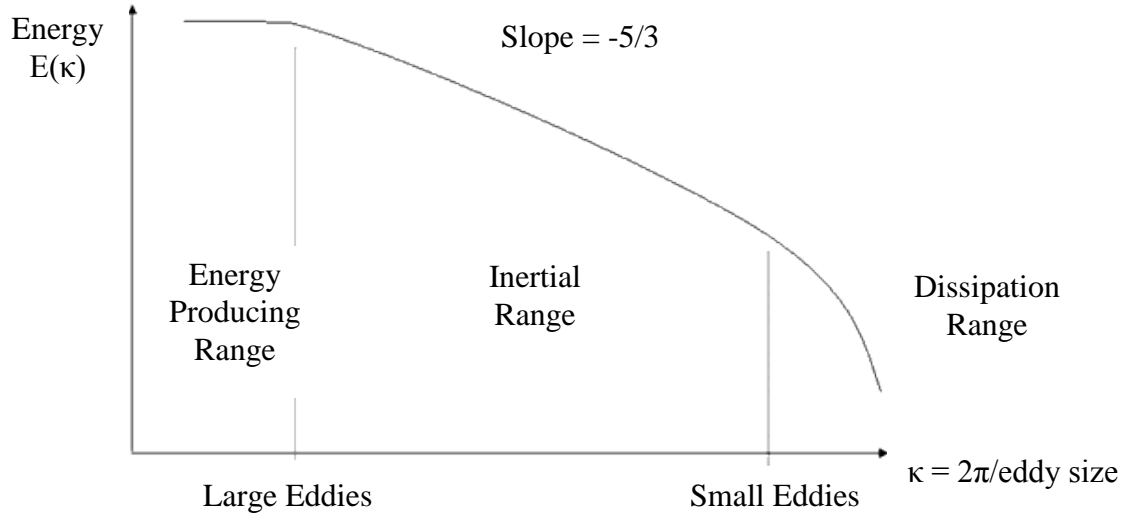
Figure 26. Kolmogorov Energy Spectrum

Determining the scale of turbulent eddy formation within the air wake is important for demonstrating the effects of the flow control fences. If the fences create a significant decrease in energy density at specific eddy sizes (typically larger or similar to the helicopter rotor diameter), it may prove favorable for helicopter operations.

Energy spectra were determined at two measurement locations, $x/H = 1.59$, $y/H = 0$, and $z/H = 0.813$ and $z/H = 1.21$. Figure 27 shows these two points of interest in the xz-plane relative to the hangar and flight deck. These points were selected based on the available anemometer test locations that matched possible flight locations for a SH-60S helicopter during shipboard launch and recovery operations. The x/H and y/H coordinates place the sampling locations nearest to the center of the YP flight deck as possible. The two vertical test locations were chosen to match the scaled height of an SH-60S when it is sitting on the flight deck and when it is in a low hover position at a quarter of a rotor diameter from the flight deck surface.
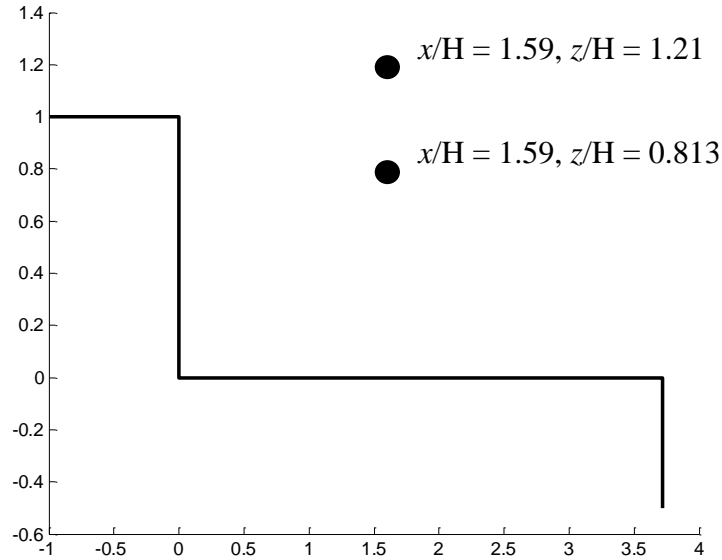
Figure 27. *In situ* time history analysis locations

Figure 28 provides the energy spectrum of the YP ship air wake with and without flow control fences at the position of $x/H = 1.59$, $y/H = 0$, and $z/H = 0.813$. For this analysis, the YP was operating in a headwind condition and velocity data was normalized using the bow reference velocity. Velocity measurements were normalized before a fast Fourier transform (FFT) was applied with 2^9 bins and 50% overlapping. The wavenumber corresponding to the hangar height is shown with a vertical arrow in the energy spectrum plots.

In the wave number domain, the flow control fences created higher turbulent kinetic energy values at a given wave number for the stream wise and cross stream wise directions (E_{11} and E_{22}). The fences produced weaker large scale eddies in the wall normal direction (E_{33}) at low wave numbers, but in the inertial range the fence and no-fence configurations produced very similar energy values. The streamwise rms velocities (u_{rms}) for the fence and no-fence

configurations at this location are 0.7204 and 0.5089, respectively. These higher u_{rms} velocities for the fence configuration confirm that the fences cause higher turbulent kinetic energy production in the streamwise direction.

The frequency domain shows the same relationship for the stream wise and cross stream wise directions with a constant shift in the log-log plot. The flow control fences created more turbulent energy in the stream wise and cross stream wise directions for a given frequency at this test location.

The flow is nearly isotropic for the fence configuration. All three flow directions (E_{11}, E_{22}, and E_{33}) collapse into each other in the inertial range, showing that there is no directionality in those eddy scales. For the no fence configuration, E_{33} deviates from the isotropic turbulence model in the inertial range. This deviation is reasonable because the wall normal direction is bounded by the flight deck surface, limiting the turbulent energy in this direction.
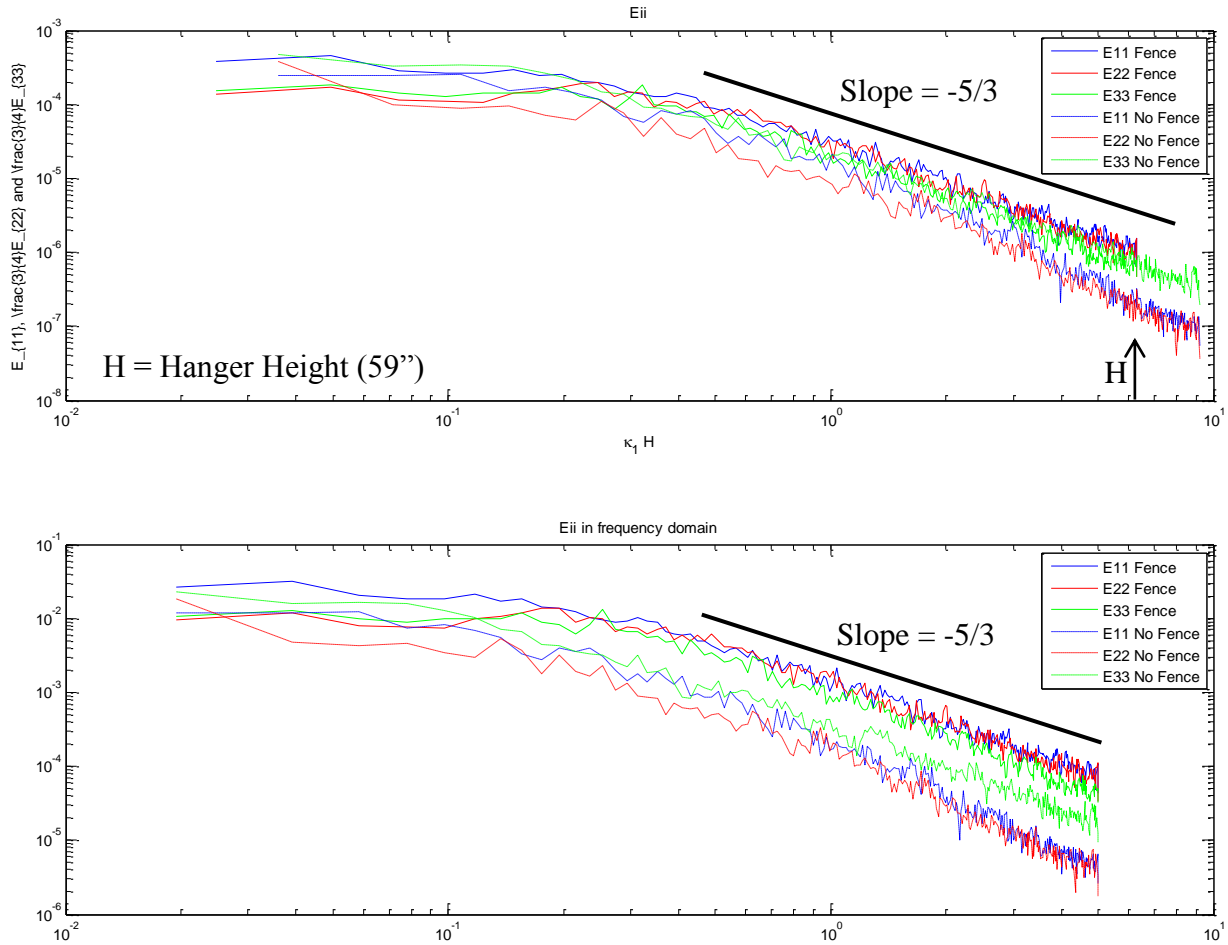
Figure 28. Energy spectrum for location x/H = 1.59, y/H = 0, and z/H = 0.813 for β = 0°

Figure 29 shows the energy spectrum for the location x/H = 1.59, y/H = 0, and z/H = 1.21. This data were also collected at a headwind condition, and velocity measurements were normalized from the bow anemometer before a fast Fourier transform was applied. In the wave number domain, the fence and no fence configurations produced similar energy levels for a given wave number in the cross stream wise (E_{22}) and wall normal direction (E_{33}). Higher energy levels were detected in the stream wise direction (E_{11}) at the beginning of the inertial range for the fence configuration. The u_{rms} values for the fence and no fence configurations are 0.8843 and

0.5683, respectively. A higher u_{rms} value for the fence configuration confirms the fences cause higher turbulent kinetic energy production in the streamwise direction.

The wave number domain shows the flow is isotropic for the fence configuration because the energy spectra for each flow direction collapse into each other during the inertial range. For the no fence configuration, the E_{33} component deviates from the isotropic turbulence model by showing slightly lower energy densities for a given wave number. Both the fence and no fence configuration have the similar turbulence length scales, with the inertial range beginning at a frequency of 0.5 Hz (wavelength of about 21 ft).
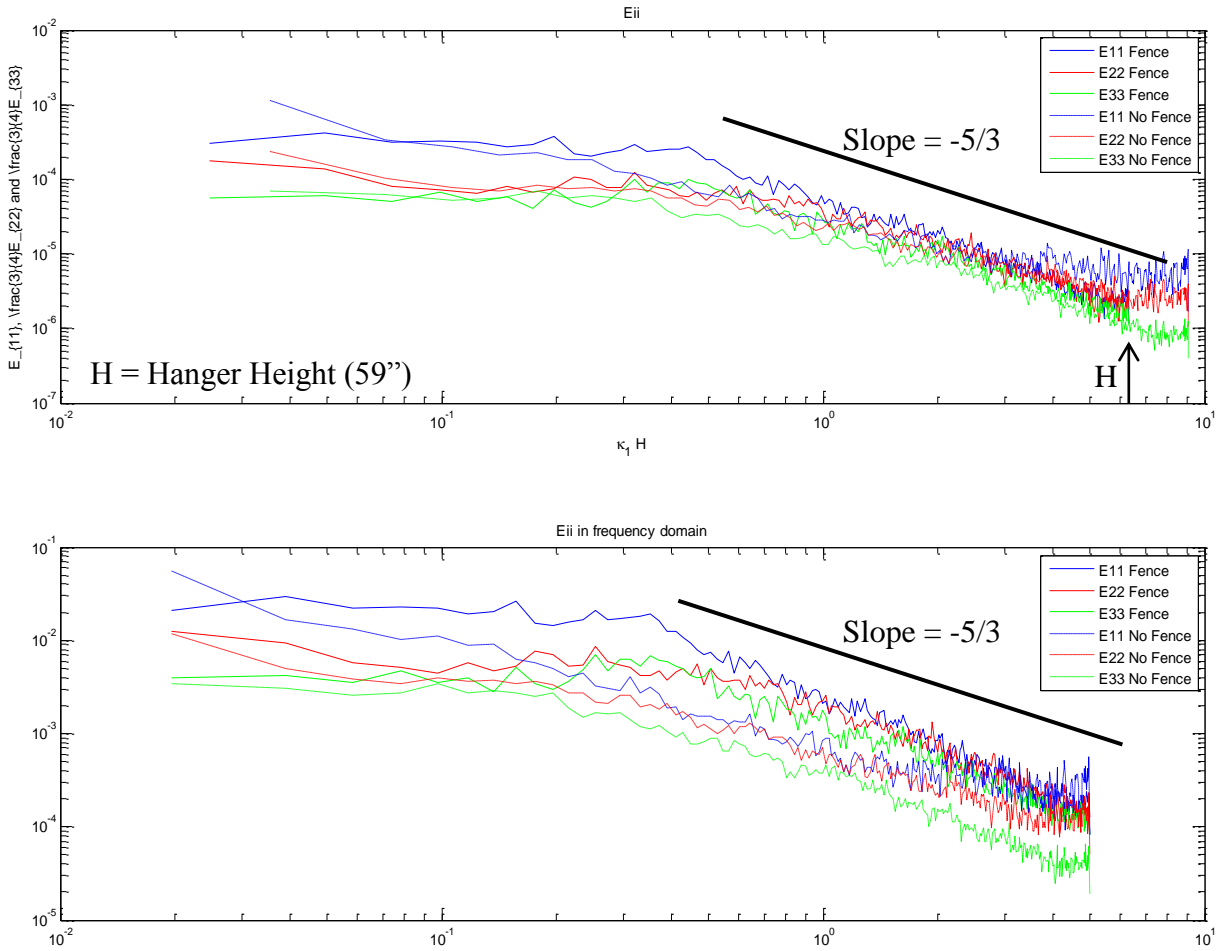
Figure 29. Energy spectrum for location x/H = 1.59, y/H = 0, and z/H = 1.21 for $\beta = 0°$

3.4.2 *Weighted Joint Probability Density Function*

A weighted joint probability density function (JPDF) of stream wise and wall normal flow can be used to describe the turbulent structures within the air wake that generate high-Reynolds shear stress. The JPDF is defined by equation (7),

$$1 = \int_{-\infty}^{\infty} P(u', w')\, du'\, dw' \tag{7}$$

Integrating the JPDF by $-u'w'$ will equal the magnitude of the mean Reynolds shear stress $-\overline{u'w'}$ as shown in equation (8),

$$-\overline{u'w'} = \int_{-\infty}^{\infty} -u'w'P(u',w')du'dw' \tag{8}$$

JPDF's were created at the two *in situ* sampling locations discussed above to investigate the effect of the fences on the turbulent mixing within the air wake.

Figure 30 contains the weighted JPDF for the fence and no fence data sets at air wake location x/H = 1.59, y/H = 0, and z/H = 0.813. The center of the JPDF for the fence data in the second and fourth quadrants has a much larger level of the cross-correlation between u' and w'. This result corresponds to the larger streamwise velocity gradient at the center of the flight deck discussed above. A larger mean velocity gradient, as shown by the JPDF, indicates there is larger Reynolds shear stress in the flow, leading to more intense and/or coherent structures in the helicopter landing region. The values of $-\overline{u'w'}$ for the fence and no fence configuration are 0.213 and 0.089, respectively. The integrated average Reynolds shear stress determined using equation (6) and the weighted JPDF in Figure 30 are 0.2104 and 0.0891 for the fence and no fence configurations, respectively. The agreement between the average and integrated values verifies the accuracy of the weighted JPDF and, more importantly, confirms that the fences create more Reynolds shear stress and larger turbulent mixing at this sampling location.
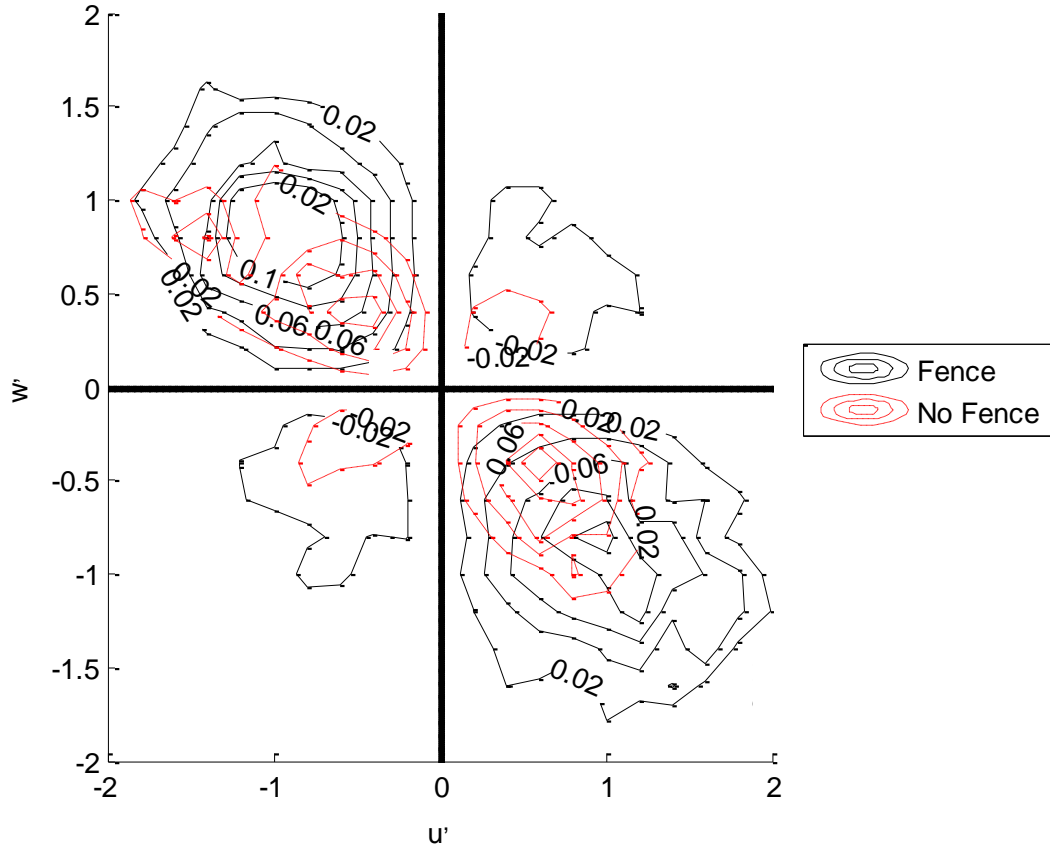
Figure 30. JPDF for location x/H = 1.59, y/H = 0, and z/H = 0.813 for β = 0°

Figure 31 shows the weighted JPDF for the location x/H = 1.59, y/H = 0, and z/H = 1.21. This JPDF also shows that the fences create higher Reynolds shear stress values within the ship air wake. The fence JPDF in the second and fourth quadrants is centered at larger u' and w' values, meaning the fences create larger Reynolds shear stress and subsequently more intense and/or coherent structures at this sampling location. The average Reynolds shear stress ($-\overline{u'w'}$) for the fence and no fence configurations is 0.304 and 0.040, respectively. The integrated average Reynolds shear stress determined using equation (6) and the weighted JPDF in Figure 30 is 0.3038 and 0.0463 for the fence and no fence configurations, respectively. Again, the

agreement between these value sets verifies the accuracy of the weighted JPDF and shows that the fences create more Reynolds shear stress and stronger turbulent mixing at the center of the flight deck.
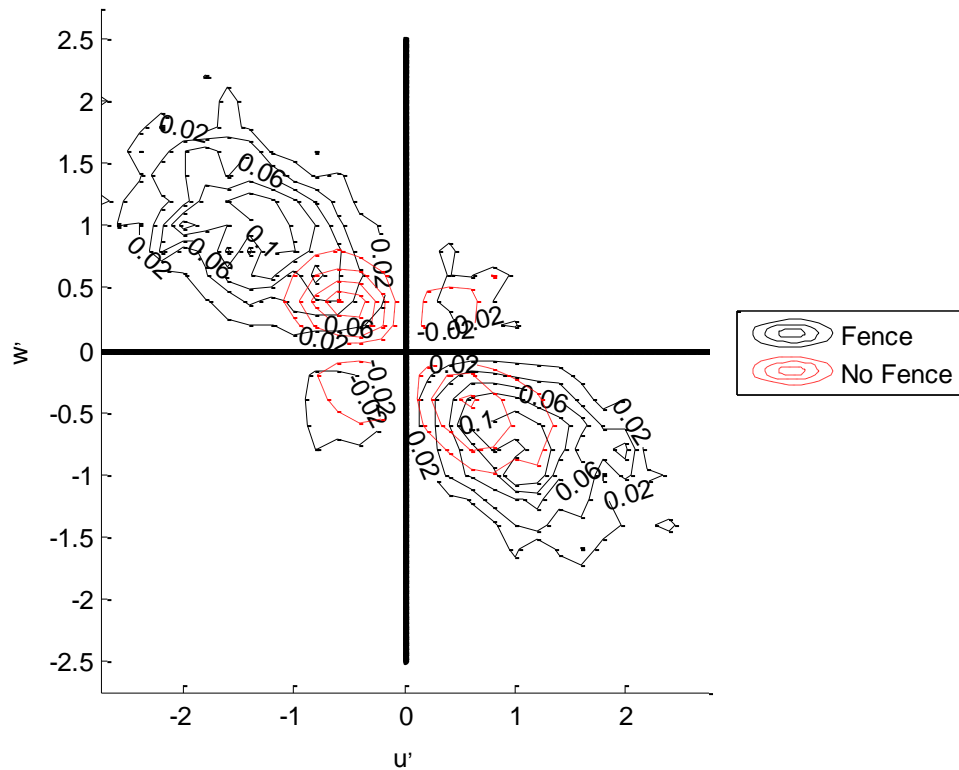
Figure 31. JPDF for location x/H = 1.59, y/H = 0, and z/H = 1.21 for $\beta = 0°$

The weighted JPDFs show the fences create larger Reynolds shear stress at the two *in situ* test locations. This result coincides with the larger mean streamwise velocity gradient discussed in the *in situ* mean velocity section above. This larger Reynolds shear stress translates to more intense and/or large coherent structures, which can be potentially hazardous to shipboard helicopter flight operations.

4 Beta 15 Results

Helicopter launch and recovery operations will often occur in crosswind conditions. For this investigation the fence design was also tested in a 15 degree crosswind from the starboard bow in order to determine the effects of passive flow control on a ship air wake generated by a crosswind. This section discusses the validity of CFD for cross wind scenarios and the effects of the flow control fences in a crosswind.

4.1 CFD Validation

Numerical simulations were run with a 20 kt uniform boundary layer inflow for the $\beta = 15°$ test condition for a Reynolds number of 23.216×10^6 based on the length of the YP. Figure 32 presents a comparison of the CFD and *in situ* measurements for the centerline plane ($y/H = 0$) at $\beta = 15°$. The plot shows agreement between the CFD and *in situ* results in both magnitude and direction. CFD predicts a slightly larger streamwise velocity gradient at the $x/H = 1$ and $x/H = 1.5$ sampling locations, but there is good agreement in velocity magnitude, direction, and streamwise velocity gradient at the other x/H test locations. This figure suggests that for the centerline plane CFD accurately predicts the streamwise flow in the air wake for the $\beta = 15°$ crosswind condition.
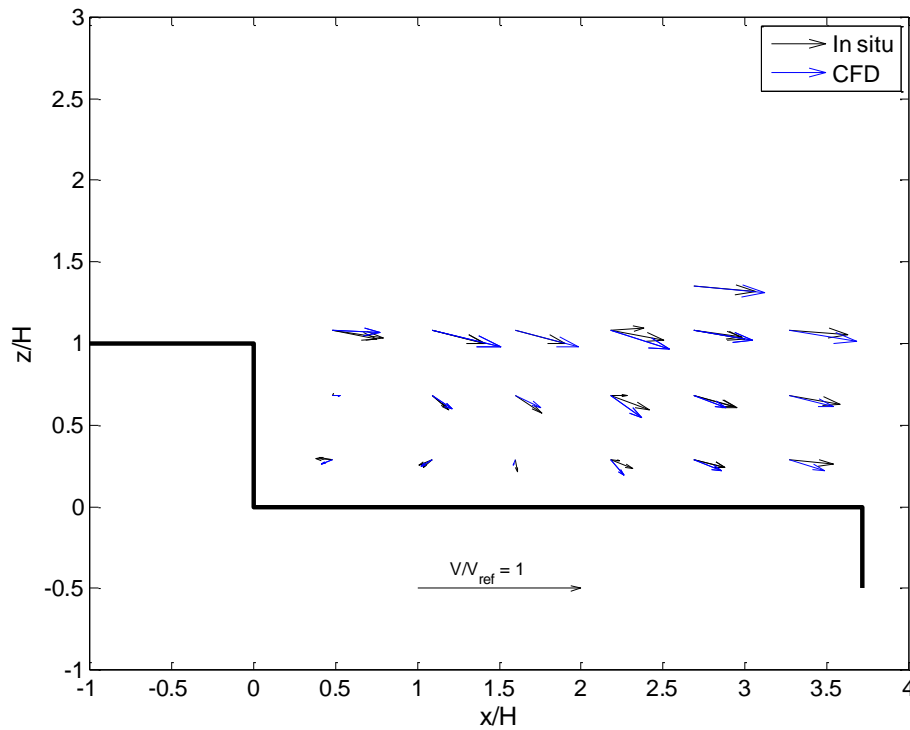
Figure 32. CFD and *in situ* data at *y*/H = 0 for β = 15°

In a crosswind it is useful to look at a horizontal slice of the air wake at a fixed test height across the entire flight deck surface to discuss the cross streamwise flow. Figure 33 shows the *in situ* measurements and CFD predictions at *z*/H = 1.08. The CFD shows a stronger cross streamwise velocity gradient with a bias towards the starboard side of the flight deck. There is poor agreement in the directionality in the cross streamwise flow, which suggests this CFD model may not provide a highly accurate cross streamwise model for the β = 15° condition.
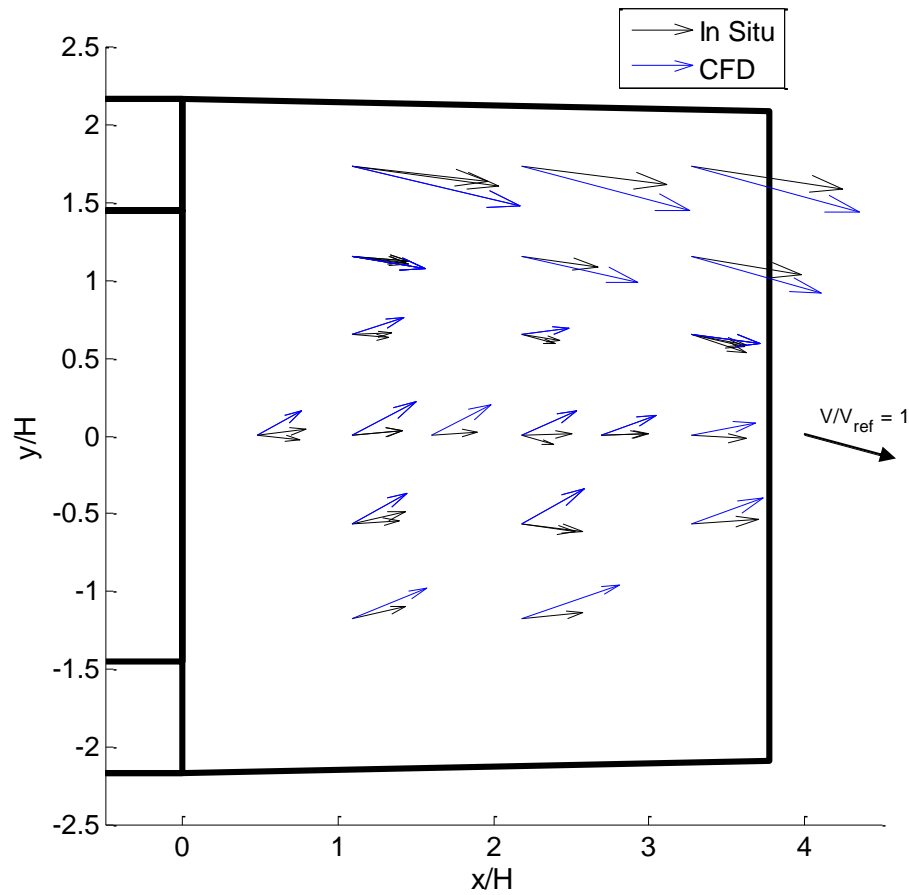
Figure 33. CFD and *in situ* data at *z*/H = 1.08 for β = 15°

CFD simulations for the β = 15° condition do not provide a highly accurate model of the ship air wake. Streamwise mean velocity flow can be used for analysis of passive flow control, but the cross streamwise results cannot be used reliably with the current CFD input parameters. Future discussion of CFD results at β = 15° only uses the streamwise and wall normal velocity components to comment on the general air wake trends observed for a crosswind, but detailed conclusions are not drawn from this data.

4.2 Flow Control Fence Analysis: Mean Velocity

4.2.1 In situ measurements

A mean velocity profile of the *in situ* measurements provides an initial qualitative analysis of the flow control fences. Figure 34 shows the air wake centerline plane of the YP for $\beta = 15°$. The fences alter the size of the recirculation zone, creating significantly more reversed flow along the centerline of the YP. In addition, the fences create a slightly larger streamwise gradient around the center of the flight deck.
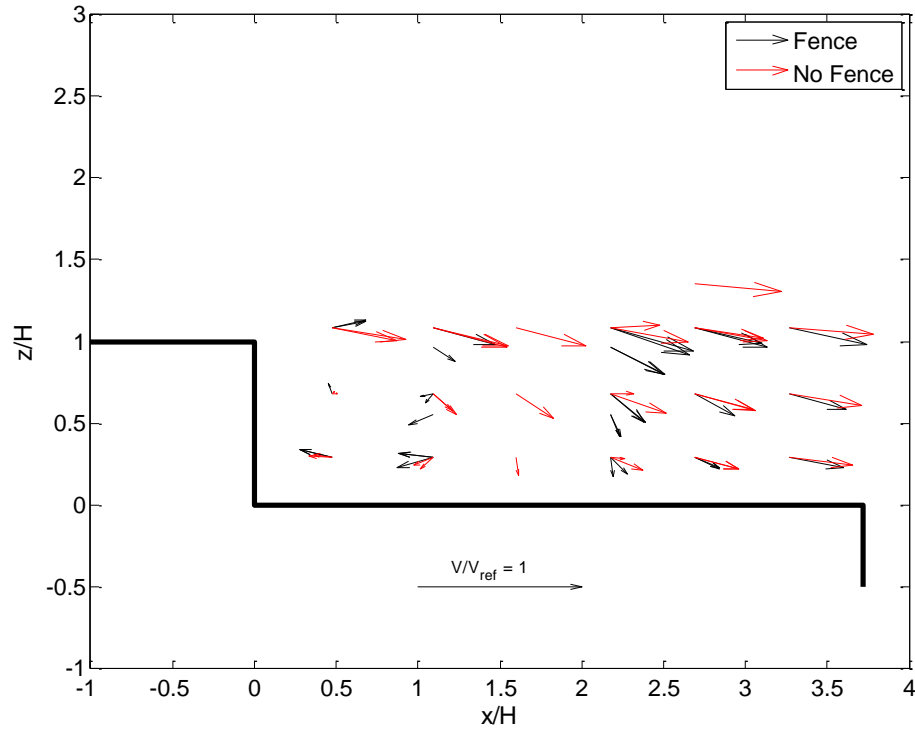
Figure 34. I*n situ* data at *y*/H = 0 for $\beta = 15°$

Figure 35 shows a horizontal plane of the air wake at *z*/H = 1.08 for the Beta 15 test condition. The plot shows that the fences do not cause a significant change in cross streamwise shear. There is good agreement in both velocity magnitude and direction for this plane.
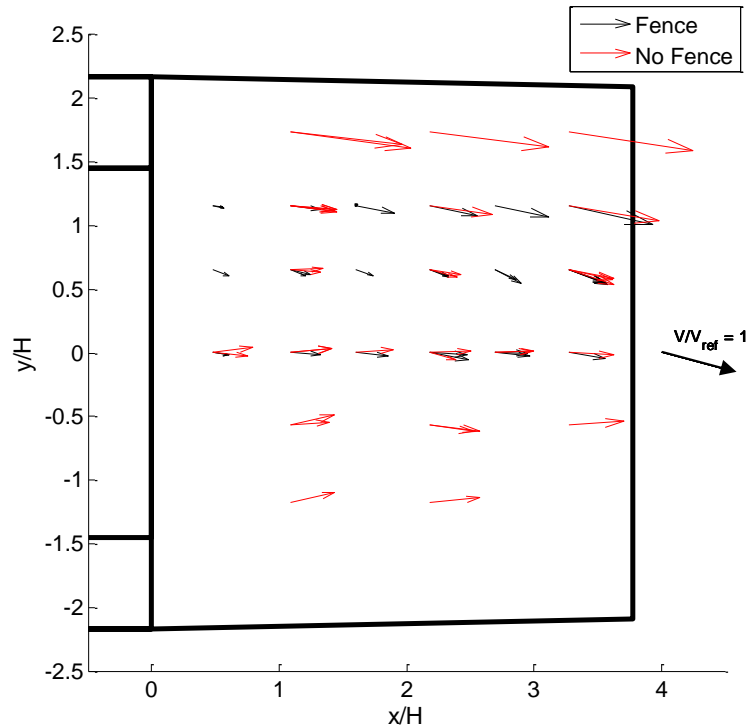
Figure 35. I*n situ* data at *z*/H = 1.08 for β = 15°

In situ mean velocity measurements show that the fences change the recirculation zone

and create more reversed flow, causing a slight increase in the streamwise velocity gradient at

the center of the flight deck. However, there is not an appreciable change in the cross

streamwise direction.

4.2.2 Computational Fluid Dynamics

The disk rotor method can be applied to the β = 15° condition to quantify the change in

downwash and velocity fluctuation levels across a disk rotor. Based on the CFD validation

discussion above, it is acceptable to use the streamwise CFD velocity data for analysis. Table 3

presents the downwash velocity and velocity standard deviation through an SH-60S rotor for the

YP in a 15 degree crosswind.   The fences create more downwash for the On Deck and Low

Hover positions, with increases of 65.8% and 217%, respectively. The fences decrease up wash

through the rotor area by 7.29% for the High Hover position and 26.25% for the High Hover Aft

position. The fences also decrease velocity fluctuation levels for the On Deck and Low Hover

locations. The High Hover position sees a slight increase in velocity fluctuation, and there is a

small but almost negligible change in velocity standard deviation for the High Hover Aft

location. These results show that the fences may cause a decrease in rotor thrust at the On Deck

and Low Hover flight positions. However the rotor area may experience less velocity

fluctuation, indicated by a lower velocity standard deviation value. For the High Hover and

High Hover Aft positions the fences could increase rotor thrust because of the decrease in up

wash through the rotor disk.

Table 3. Downwash velocity w and standard deviation σ for CFD simulations at $\beta = 15°$

Position	Fence		No Fence	
	w (ft/s)	σ	w (ft/s)	σ
On Deck	-2.4395	3.1564	-1.4713	3.4499
Low Hover	-0.7321	3.1437	0.6236	3.3904
High Hover	2.0434	3.0781	2.2040	2.8947
Aft Hover	2.2476	2.9207	3.0475	2.9159

4.2.3 Wind tunnel experiments

Mean velocity and vorticity measurements from wind tunnel experiments can be used to

discuss the effects of the flow control fences. Figure 36 shows the mean velocity distribution at

x/H = 1.504 for the fence and no fence configurations. There is not a noticeable change in the

size or magnitude of the cross streamwise velocity gradients. In addition, the fences did not

cause any movement of the vortex centered at $y/H = -0.55$ and $z/H = 1.7$.
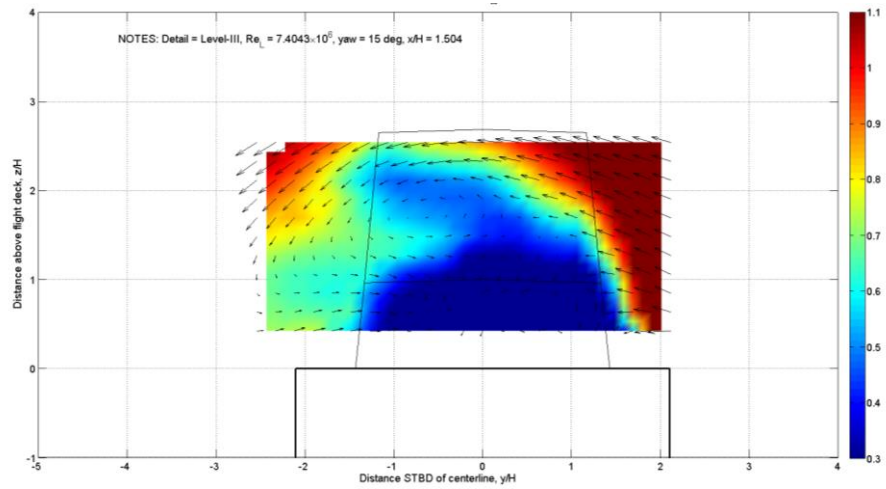
a) Fence
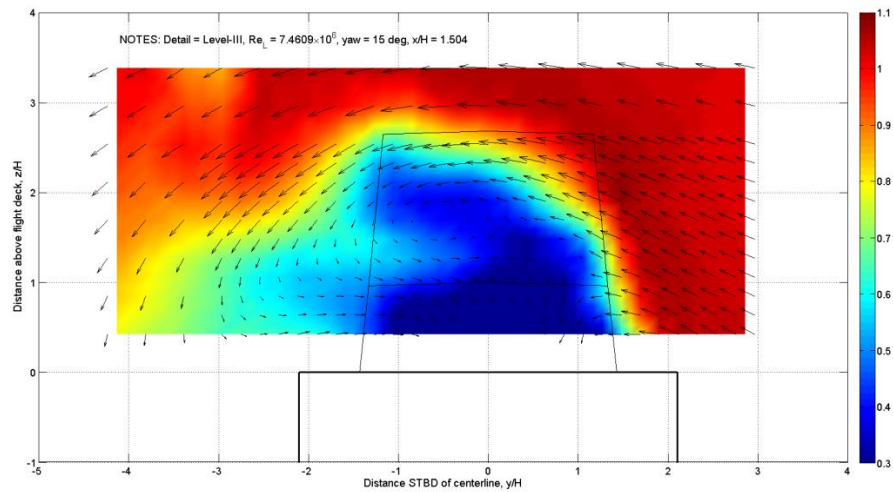
b) No Fence

Figure 36. Mean velocity profile for $\beta = 15°$ at $x/H = 1.504$: a) fence, b) no fence configuration

Figure 37 presents the vorticity measurements of the air wake at $x/H = 1.504$ for the fence

and no fence configurations. The fences generated more vorticity below $z/H = 1$, which

corresponds to the increase in the streamwise velocity gradient discussed above. The fences also

caused vorticity to increase at $z/H = 2$. A region of reduced vorticity developed at $z/H = 1.3$, which may be problematic for helicopter operations because larger changes in vorticity could lead to higher pilot workload to maintain a steady heading and position over the flight deck.
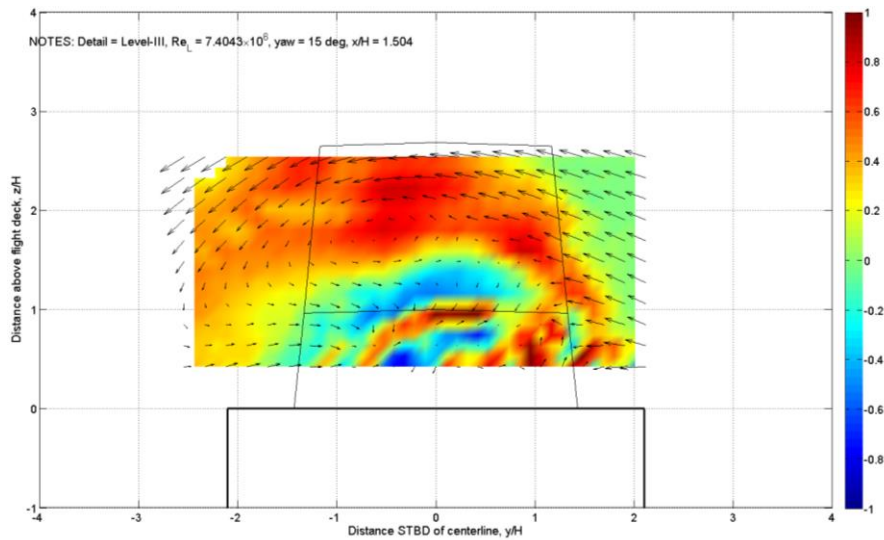
a) Fence
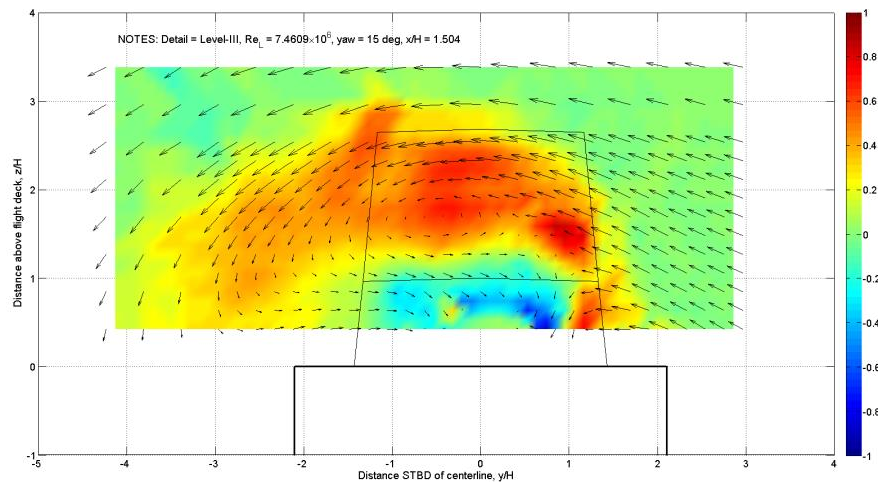
b) No Fence

Figure 37. Vorticity comparison for $\beta = 15°$ at $x/H = 1.504$: a) fence, b) no fence configuration

4.3 Flow Control Fence Analysis: Turbulence Statistics

In situ time history analysis using the energy spectra and weighted joint probability function methods described above can be used for the $\beta = 15°$ test condition. The location of interest is $x/H = 1.59$, $y/H = 0$, and $z/H = 0.77$. The sampling locations for $\beta = 0°$ and $\beta = 15°$ could not be matched exactly so the sampling location for $\beta = 15°$ analysis was chosen based on the closest possible test height producing sufficient data to accurately create an energy spectrum and a weighted JDPF.

4.3.1 Energy Spectrum

Figure 38 shows the energy spectrum for the location $x/H = 1.59$, $y/H = 0$, and $z/H = 0.77$. The fences produce higher energy levels in the stream wise direction (E_{11}) and lower energy levels for the cross stream wise and wall normal directions (E_{22} and E_{33}) for the largest turbulent structures in the flow. In the inertial range there is little difference in energy levels between the fence and no fence configurations for all wave numbers. The u_{rms} values for the fence and no fence configuration are 0.5254 and 0.5822 respectively. These values suggest there is a slightly larger energy density in the E_{11} direction for the no fence configuration, but the difference in streamwise turbulent kinetic energy is not as significant for a crosswind as for the $\beta = 0°$ condition. The flow is nearly isotropic for both configurations, with a small deviation in the E_{33} component from the isotropic turbulence model.
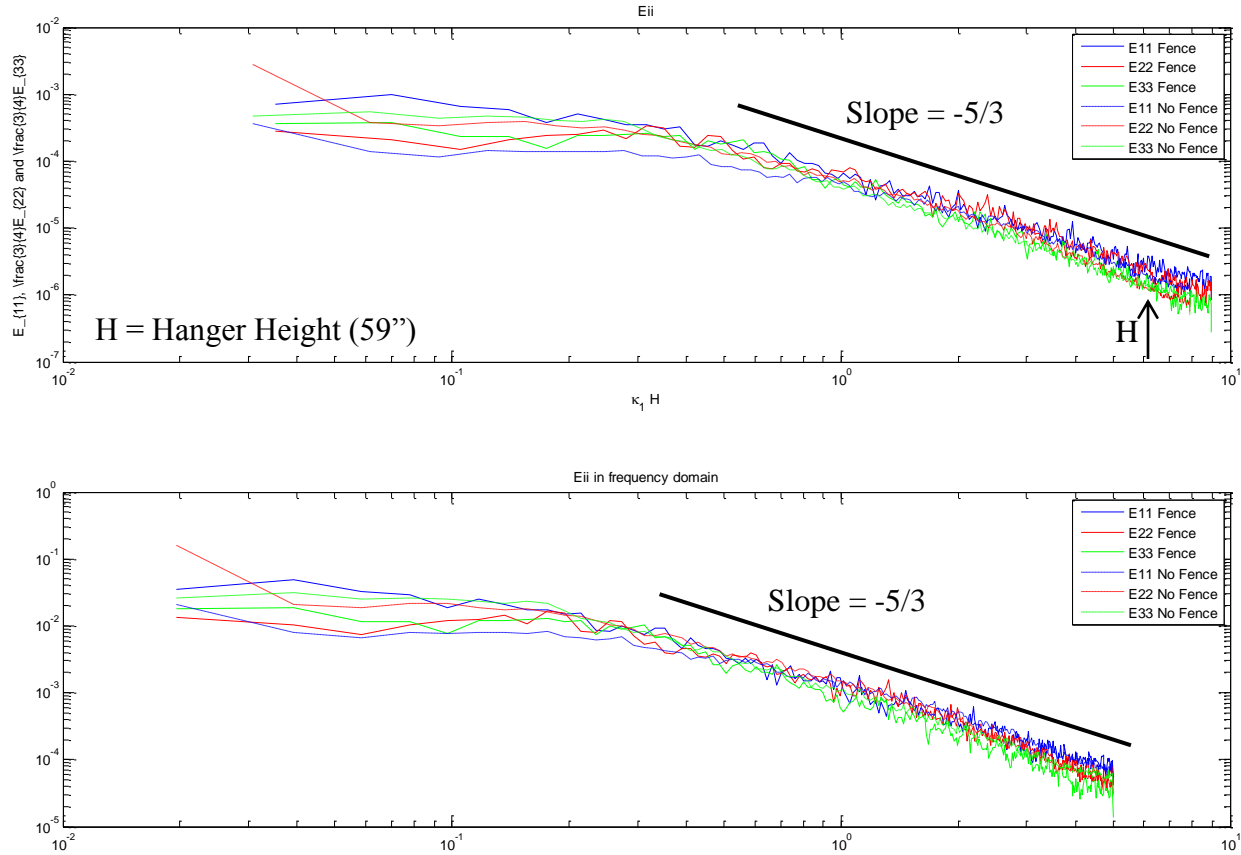
Figure 38. Energy spectrum for location $x/H = 1.59$, $y/H = 0$, and $z/H = 0.77$ for $\beta = 15°$

4.3.2 Joint Probability Density Functions

Figure 39 shows the weighted joint probability density functions for the location $x/H = 1.59$, $y/H = 0$, and $z/H = 0.77$ for $\beta = 15°$. The figure shows that there is a similar Reynolds shear stress distribution for the fence and no fence configurations because both JPDF's are centered at the same $u'w'$ location in the second and fourth quadrant. The average Reynolds shear stress ($-\overline{u'w'}$) for the fence and no fence configurations is 0.114 and 0.111, respectively. The integrated average Reynolds shear stresses from Equation (6) are 0.1143 and 0.1109, for the fence and no fence configurations, respectively. These pairs of values verify the accuracy of the

weighted JPDF, and show that the fences did not cause a significant change in the turbulent

mixing of the air wake for the β = 15° condition.
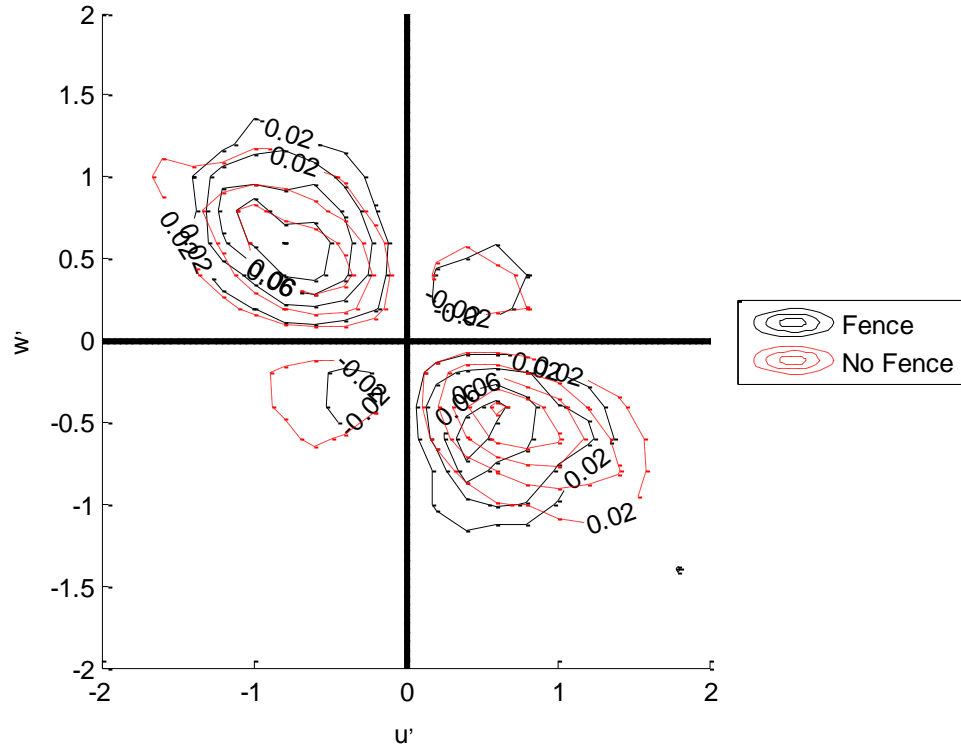
Figure 39. JPDF for location *x*/H = 1.59, *y*/H = 0, and *z*/H = 0.77 for β = 15°

In situ time history data shows that the fences do not create a significant increase in the

turbulent kinetic energy or Reynolds shear stress (turbulent mixing) of the flow. There is a

slightly larger streamwise velocity gradient in the helicopter landing region, but the second order

turbulent nature of the flow does not show a significant change in the potentially hazardous air

wake flow structures.

5 Conclusions

This research leads to two primary conclusions. The first explores the changes in the air wake caused by the addition of the flow control fences. The second concerns the usefulness of CFD for predicting ship air wake changes due to the addition of different flow control devices.

Numerical simulations, wind tunnel experiments, and *in situ* measurements all produce the same general conclusions about the flow control fence tested in this investigation. The flow control fences changed the ship air wake for the $\beta = 0°$ condition in the following ways:

- Recirculation zone growth and aft movement of the reattachment point

- Disk rotor analysis shows that the fences cause downwash to decrease for the on deck, low hover, and high hover flight positions.

More detailed analysis of *in situ* measurements showed the following effects of the fences on the YP air wake:

- Larger streamwise velocity gradient at the center of the flight deck

- Larger streamwise flow velocity fluctuation levels (u_{rms}) at hangar height

- Higher turbulent kinetic energy production at the center of the flight deck

- Larger Reynolds shear stress at the center of the flight deck

- Stronger mixing created by fences at the center of the flight deck

Changes in mean velocity will affect rotor thrust produced by a helicopter, and the increase in velocity fluctuation levels may have an effect on perceived pilot workload due to a

wider spectrum of wind velocities the rotor could encounter in unsteady conditions. Higher turbulent kinetic energy and larger Reynolds shear stress can create stronger eddies (recirculating flow) at the center of the flight deck. This result could potentially lead to higher pilot workload during launch and recovery operations because a pilot would have to negotiate through a region of stronger rotational flow that may impose larger aerodynamic forces on the helicopter.

For $\beta = 15°$, the fences created a slightly larger streamwise velocity gradient but did not have a significant effect on the cross streamwise flow. There was not a significant increase in turbulent kinetic energy or Reynolds shear stress at the center of the flight deck. These results suggest that the fences altered the size and shape of the recirculation zone but did not have an effect on the second order turbulent nature of the air wake (negligible change in turbulent kinetic energy and Reynolds shear stress).

This investigation also showed the limitations of CFD in modeling a ship air wake. Numerical simulations did not accurately model the mean velocity flow field of the air wake. CFD predicted a larger streamwise velocity gradient and higher streamwise velocity fluctuation levels than the *in situ* measurements. However, CFD was able to show that the recirculation zone grew and the reattachment point moved aft. Future studies could employ CFD as a first-step analysis tool to compare a wide variety of passive flow control devices, but final conclusions about a particular device's effectiveness should not be developed without wind tunnel and *in situ* validation.

Future research for ship air wake passive flow control could include adding a helicopter rotor in CFD simulations and/or full scale testing to determine the effects of rotor downwash on a ship air wake. The presence of helicopter rotor downwash will change the ship air wake and

may alter the effectiveness and importance of passive flow control. Additionally, CFD simulations could be supplemented by a more accurate inflow condition that matches the streamwise velocity distribution and turbulence parameters of the atmospheric boundary layer of the Chesapeake Bay. Finally, flight testing with a remote control helicopter could be performed to determine the relationship between changing each ship air wake parameter and improving the flow for launch and recovery operations.

R e f e r e n c e s

[1]   "Helicopter operating procedures for air-capable ships NATOPS manual," NAVAIR 0008T-122, 2003.

[2]   Snyder, M.R., and Kang, H.S., "Comparison of Experimental and Computational Ship Air Wakes for YP Class Patrol Craft," *AIAA 2011-7045: Centennial of Naval Aviation Forum "100 Years of Achievement and Progress,"* Virginia Beach, VA, 21-22 September, 2011.

[3]   Guillot, M.J., "Computational simulation of the air wake over a naval transport vessel," *AIAA Journal*, 40(10), 2002.

[4]   Lee, D., Sezer-Uzol, N., Horn, J.F., and Long, L.N., "Simulation of helicopter ship-board launch and recovery with time-accurate airwakes," *Journal of Aircraft*, 42(2), March-April 2005.

[5]   Geder, J., Ramamurti, R., and Sandberg, W.C., "Ship airwake correlation analysis for the San Antonio Class Transport Dock Vessel," *Naval Research Laboratory paper MRL/MR/6410-09-9127*, 21 May 2008.

[6]   Driver, D. M., Seegmiller, H. L., and Marvin, J. G., "Time-Dependent Behavior of a Reattaching Shear Layer", *AIAA Journal*, Vol 25, No. 7, pp. 914-919, 1987.

[7]   Rhoades, Mark M., "A Study of the Airwake Aerodynamics Over the Flight Deck of an AOR Model Ship", MS Thesis, Naval Postgraduate School, Monterey, CA, Sept. 1990.

[8]   Johns, Michael K., "Flow Visualization of the Airwake around a Model of a DD-963 Class Destroyer in a Simulated Atmospheric Boundary Layer", MS Thesis, Naval Postgraduate School, Monterey, CA, Sept. 1988.

[9]   Sharma, A., and Long, L.N., "Airwake Simulations on an LPD 17 Ship," *AIAA 2001-2589: 15th AIAA Computational Fluid Dynamics Conference,* Anaheim, California, 2001.

[10]   Shafer, D.M., "Active and Passive Flow Control over the Flight Deck of Small Naval Vessels", MSc Thesis, Virginia Polytechnic Institute, April 2005.

[11]   Greenwell, D.I., and Barrett, R.V., "Inclined Screens for Control of Ship Air Wakes," *AIAA 2006-3502: 3rd AIAA Flow Control Conference, San Francisco, California*, 5-8 June 2006.

[12]   Narveson, Marshall, L., "Flow Modification over a Backward Facing Step," Thesis, Naval Postgraduate School, September, 1990.

[13]   Woolman, Scott, G., "Control of Flow Over a Backward Facing Step," Thesis, Naval Postgraduate School, September, 1990.

[14]   Snyder, M.R., Shishkoff, J.P., Roberson, F.D., McDonald, M.C., Brownell, C.J., Luznik L., Miklosovic, D.S., and Burks, J.S., "Comparison of Experimental and Computational Ship Air Wakes for YP Class Patrol Craft," American Society of Naval   Engineers Launch and Recovery Symposium, Arlington, VA, December 2010.

[15]   Polsky, S., Imber, R., Czerwiec, R., & Ghee, T., "A Computational and Experimental Determination of the Air Flow Around the Landing Deck of a US Navy Destroyer (DDG): Part II," *AIAA-2007-4484: 37th AIAA Fluid Dynamics Conference and Exhibit*, Miami, Florida, 2007.

[16]   Snyder, M.R., Kang, H.S., Brownell, C.J. and Burks, J.S., "Validation of Ship Air Wake Simulations and Investigation of Ship Air Wake Impact on Rotary Wing Aircraft," American Society of Naval Engineers Launch and Recovery Symposium, Linthicum, MD, November 2012.

[17]   Miklosovic, D. S., Kang, H.S., Snyder, M. R., "Ship Air Wake Wind Tunnel Test Results," *AIAA 2011 3155: 29th AIAA Applied Aerodynamics Conference*, Honolulu, Hawaii, 2011.

[18]   Bramwell, A.R.S., Done, G. and Balmford, D., "*Helicopter Dynamics*", 2nd Edition, Butterworth-Heinemann, Oxford, 2001, Chapters 4 & 5.

APPENDIX A: Raw Data Examples

Sample *in situ* data

File	# Anem	Bow	Beta	#line	Boat Speed	
2	3	1	0.0	13996	9.0	

Anem	x (m)	y (m)	z (m)	+U	+W
1	-28.403	0.000	3.095	A	D
2	2.360	0.025	1.020	A	U
3	4.090	1.750	1.010	A	U

T(C)	P(hPa)	RH(%)
24.0	1020.0	57.0
24.0	1020.0	57.0

YYYY MM DD HH MM SS(Time)
2012 10 05 09 04 11

```
10.80  2.04  0.96 -0.32  0.09 -0.21  1.43 -1.11  0.05
10.87  2.14  0.89 -0.51  0.24  0.07  1.29 -0.66 -0.04
11.02  2.40  0.63 -0.35  0.23  0.15  1.77  0.17  0.05
10.95  2.48  0.64  0.02  0.86  0.24  1.51  0.44  0.28
10.77  2.56  0.75  0.11  0.86 -0.18  1.42  0.20 -0.46
10.84  2.49  0.80  0.57  0.53 -0.34  2.06 -0.37 -0.21
10.83  2.50  0.89  0.84  0.31 -0.37  2.34 -0.49 -0.52
10.83  2.57  1.06  0.76  0.19 -0.44  2.50 -0.79  0.91
10.88  2.37  0.80  0.69  0.28 -0.59  3.12 -1.28  0.88
10.86  2.41  0.79  0.93  0.08 -0.88  2.80 -0.93 -0.36
10.92  2.60  0.98  0.87  0.45 -0.77  2.38 -1.69 -1.52
10.87  2.64  0.95  0.55  0.32 -0.52  1.94 -0.44 -0.12
11.05  2.41  0.82  0.11  0.43 -0.53  1.49  1.28 -0.02
11.08  2.09  0.79 -0.86  0.42  0.09  1.29  0.95 -0.61
10.79  2.23  0.84 -1.65  0.11  0.80  1.53  0.59 -0.50
10.79  2.24  0.99 -1.33 -0.77 -0.32  1.46  0.53 -0.27
10.94  2.70  0.78 -1.74 -0.80  0.35  1.49  0.41 -0.19
10.95  3.17  0.66 -0.99 -0.39 -0.42  0.84 -0.89 -0.33
11.30  2.74  0.60 -0.22 -0.44 -1.25  1.17 -1.36 -0.59
11.25  2.57  0.67  0.42 -0.96 -0.73  2.25 -0.82  0.23
11.27  2.51  0.89  0.46 -2.09 -0.62  2.03 -0.85  0.65
11.37  3.01  0.95  0.25 -1.95 -0.61  2.13 -0.94 -0.30
10.99  2.83  0.95 -0.53 -2.44  0.24  2.45 -1.28 -0.23
10.82  2.71  0.91  0.08 -1.49  0.11  1.70 -0.97  0.90
10.77  2.26  1.04  0.08 -1.44  0.37  1.06 -0.92  1.25
10.92  2.33  0.93 -0.10 -1.57  0.14  2.54 -1.20  0.21
```

APPENDIX B: MATLAB Scripts

Plot mean velocity profile (PFC_Comparison_V3.m)
The input section of this code has been included to show the various options available for plotting the ship air wake data. This code can display data any combination of CFD, wind tunnel, and underway measurements with different yaw angles, boundary layer profiles, inflow speeds.

```matlab
%% Ship Airwake Data Analysis for Passive Flow Control
% Based on PFC_Comparison_V2 cose
% Written 17 January 2013 by Nick LaSalle
%
% This code can plot underway, wind tunnel, and CFD results on longitudinal
% planes.  The input section at the top of the code sets the data locations
% and allows the user to set the yaw angle and the desired data sets to plot

clear, clc, format compact, close all;

%% Input

% Set yaw angle (3 digit format - 000, 015)
yaw = 000;
beta = '000';

% Select fences or no fence data
% 1 = fence data only, 2 = no fence data only, 3 = fence and no fence data
fence = 1;

% Select data sets you want to plot
% 1 = underway only, 2 = CFD only, 3 = WT only, 4 = underway+CFD,
% 5 = underway+WT, 6 = CFD+WT, 7 = all
dataType = 1;

% Select desired plot plane
% 1 = y plane (longitudinal), 2 = z plane
plane = 1;

% Select CFD boundary layer input - ABL or Uniform
%BL = 'ABL';
BL = 'UNI';

% Set speed for CFD data (7,12,15,20 knots)
speed = '20';
```

Create Locations for Disk Method Analysis (createDiskLocations.m)

```matlab
%% Make point disk cloud for helicopter rotor analyis
% Written by Nick LaSalle
% 3 Feb 2013

% Disk will be used to integrate mean and standard deviation across rotor
disk
% Used scaled rotor diameters for SH-60 and Firescout helicopter, scaled from
area of
% rotor versus area of flight deck on DDG.

%% Sizing

% DDG Flight IIA flight deck/hangar dimensions
DDGArea = 0.5*71*(57+44); %ft^2
DDGHangarH = 20; %ft

% YP 676 flight deck dimensions
YPArea = 0.5*223/12*(256/12+247/12);
YPHangarH = 59/12; %ft

% Helo heights
HeloHeight = [17+2/12,9.71,1.15814]; %ft, SH-60S, Firescout, TRex 600

% Scale helo heights
HeloHeightScaled = YPHangarH * (HeloHeight/DDGHangarH);

%% Set parameters

% Set rotor helicopter to use
% 1 = SH-60S, 2 = Firescout, 3 = T-Rex 600 R/C Helo
helo = 1;

% Number of azimuth angles
theta = 32;

% Number of points per radius
numRadius = 15;

for w = 1:4
    % Set helo position: 1 = on deck, 2 = low hover (1 rotor diameter), 3 =
high hover (2.5 rotor diameters), 4 = high
    % hover over aft edge of flight deck
    position = w;
    switch position
        case 1
            positionName = 'OnDeck';
        case 2
```

```matlab
            positionName = 'LowHover';
        case 3
            positionName = 'HighHover';
        case 4
            positionName = 'HighHoverAft';
end

% Set center location for cloud disk
% Flight deck length = 18.5833 ft
% Flight deck width = 21.3333 ft at hangar, 20.5833 ft at aft edge
% Hangar height =  59 inches = 4.9167 ft.

% Positions 1-3 at centerline and halfway between hangar and aft end of
% YP flight deck, position 4 at centerline and aft end of flight deck
if position == 4
    xCenter = 18.5833; %ft, aft edge of flight deck
else
    xCenter = 18.5833/2; %center of flight deck
end
yCenter = 0; %ft, 0 = centerline

% Helicopter rotor diameters
switch helo
    case 1
        rotor = 53 + 8/12; %ft, SH-60S
        heloName = 'SH60S';
        rotorScaled = YPHangarH * (rotor/DDGHangarH); %scale rotor ft
    case 2
        rotor = 27.5; % ft, Firescout
        heloName = 'Firescout';
        rotorScaled = YPHangarH * (rotor/DDGHangarH); %scale rotor ft
    case 3
        rotorScaled = 4.429; %ft, T-Rex 600
        heloName = 'TRex';
end

switch position
    case 1
        zCenter = HeloHeightScaled(helo); %ft
    case 2
        zCenter = HeloHeightScaled(helo) + rotorScaled;
    case 3
        zCenter = HeloHeightScaled(helo) + 2.5*rotorScaled;
    case 4
        zCenter = HeloHeightScaled(helo) + 2.5*rotorScaled;
end

% CFD offsets
xoff_CFD = 86.0;  % ft from the leading edge to the deck in x
yoff_CFD = 0;
zoff_CFD = 9.194;   % ft, deck height from the sea level
```

```matlab
    %% Create points cloud based on azimuths and concentric circles

    azimuth = zeros(theta,1);
    % Create azimuth angles
    for i = 1:theta
        azimuth(i) = 360/theta*i;
    end

    radSpacing = (rotorScaled/2)/numRadius;

    diskPoints = zeros(1 + theta*numRadius,4);

    diskPoints(1,1) = xCenter;
    diskPoints(1,2) = yCenter;
    diskPoints(1,3) = zCenter;
    diskPoints(1,4) = 1000;

    count = 2;
    for j = 1:theta
        for k = 1:numRadius
            diskPoints(count,1) = xCenter - k*radSpacing*cosd(azimuth(j));
            diskPoints(count,2) = yCenter + k*radSpacing*sind(azimuth(j));
            diskPoints(count,3) = zCenter;
            diskPoints(count,4) = azimuth(j);
            count = count + 1;
        end
    end

    % Convert from hangar relative coordinates to CFD coordinates
    diskPoints(:,1) = diskPoints(:,1) + xoff_CFD;
    diskPoints(:,2) = diskPoints(:,2) + yoff_CFD;
    diskPoints(:,3) = diskPoints(:,3) + zoff_CFD;

    % Write to text file
    path = 'F:\LaSalle Trident\Airwake Analysis\Disk Analysis\';
    fname = [path,'diskLocations_',heloName,'_',positionName,'.txt'];
    fid = fopen(fname,'w');
    fprintf(fid,'#Version 1.0\r\n');
    fprintf(fid,'#EnSight Point Format\r\n');
    for i = 1:count-1
        fprintf(fid,'%1.6f,',diskPoints(i,1));
        fprintf(fid,'%1.6f,',diskPoints(i,2));
        fprintf(fid,'%1.6f\r\n',diskPoints(i,3));
    end
    fclose(fid);
end

%% Calculate Point Density
rotorArea = pi*rotorScaled^2;
numPoints = 1 + theta*numRadius;
rotorDensity = numPoints/rotorArea; %points per square foot of rotor area
```

```
disp(num2str(rotorDensity));
```

Disk Method Reduction Code (diskAnalysis.m)

```
%% Disk Analysis
% Written by Nick LaSalle
% 3 Feb 2012

% This script integrates the mean and standard deviations of the flow field
% across the helicopter rotor region created using the
% "createDiskLocations" script

clear, clc, format compact, close all;

%% Set input parameters

% Set helo rotor to be analyzed
% SH60S, Firescout, TRex
helo = 'SH60S';

% Set fence or no fence data
%Fence = 'Fence';
Fence = 'NoFence';

% Set boundary layer
BL = 'UNI';

% Set speed
speed = '20';

%% Read data and integrate across rotor
downwash = zeros(4,2);

for i = 1:4

    switch i
        case 1
            position = 'OnDeck';
        case 2
            position = 'LowHover';
        case 3
            position = 'HighHover';
        case 4
            position = 'HighHoverAft';
    end

    % Read data
    fpath_disk_in  = ['F:\LaSalle Trident\Airwake Analysis\Disk
Analysis\',helo,'\'];
```

```matlab
    fname_disk_in  =
['diskResults_',helo,'_',position,'_',BL,'_',Fence,'_',speed,'kt.flat'];
    fpath_disk_out = ['F:\LaSalle Trident\Airwake Analysis\Disk
Analysis\',helo];

    % Open and read the flat file.
    A = importdata([fpath_disk_in, fname_disk_in]);
    data = A.data;

    numPoints = length(data(:,1));

    loc = data(:,1:3);
    vel = data(:,4:6);
    STD = data(:,7:9);

    % Normalize velocity and STD components


    % Integrate across rotor disk
    % Integrate Z velocity component (mean downwash across rotor)
    downwash(i,1) = mean(vel(:,3));
    downwash(i,2) = mean(STD(:,3));

end

% Write to excel file
excelName = ['C:\LaSalle Trident\Airwake Analysis\Disk
Analysis\',helo,'\',helo,'_',Fence,'_reducedDownwash.xls'];
xlswrite(excelName,downwash);
```

Joint Probability Density Function Creator (PFC_Anem_Stat.m)

```matlab
%***********************************************************************
%                                                                      *
%         Statistics program for SAW underways                         *
%             from sonic anemometers.                                  *
%                                                                      *
%                               Hyung Suk Kang                         *
%                                August 30, 2010                       *
%                                                                      *
%                             Updated by Nick LaSalle                  *
%                               Jan - March 2013                       *
%                                                                      *
%         Reference: Numerical Recipes                                 *
%                                                                      *
%***********************************************************************

clc,clear,format compact

% Number of files is for Fence data
beta='000';
yaw = 000;
%beta=-15; nfile=23;    %Make sure the real beta is negative

path = ['F:\LaSalle Trident\Underways\Fence\beta',beta,'\'];
project = 'PFC';
pathNF = ['F:\LaSalle Trident\Underways\NoFence\beta',beta,'\'];
projectNF = 'SAW';

% PDF Parameters
ifile = 52;
probe = 4;
ifileNF = 63;
probeNF = 8;
nt = 20;
du = 0.2;
dw = du;

%% Run JPDF for fence data
% Num files for fence data
nfile=54;

% Get file info
[loc nprobe ndata cont temp press
humid]=read_logc_file(path,project,beta,nfile);
```

```matlab
[u v w
T]=PFC_read_velocity_data_file(path,project,beta,ifile,ndata(ifile),nprobe(if
ile));

%[yaw,pitch] = yaw_pitch_angle(ndata,u,v,w);

[nbin ibegin iend
nvalid]=find_valid_data_chunks(1,yaw,ifile,ndata(ifile),u,v,w);

%running_average(yaw,ndata,nprobe,ifile,u,v,w,nbin,ibegin,iend)

[meanu(1:nprobe(ifile)),meanv(1:nprobe(ifile)),meanw(1:nprobe(ifile)),...
        uu(1:nprobe(ifile)),vv(1:nprobe(ifile)),ww(1:nprobe(ifile)),...

uv(1:nprobe(ifile)),vw(1:nprobe(ifile)),wu(1:nprobe(ifile)),ke(1:nprobe(ifile
)),...
        Su(1:nprobe(ifile)),Sv(1:nprobe(ifile)),Sw(1:nprobe(ifile)),...
        Fu(1:nprobe(ifile)),Fv(1:nprobe(ifile)),Fw(1:nprobe(ifile))]=...
        moment_valid(ndata(ifile),nprobe(ifile),nbin,ibegin,iend,u,v,w);

Ubow = meanu(1);

% Find velocity fluctuations
uf = zeros(nprobe(ifile),length(u));
vf = zeros(nprobe(ifile),length(v));
wf = zeros(nprobe(ifile),length(w));
for ip=1:nprobe(ifile)
    uf(ip,:) = u(:,ip)' - meanu(ip);
    vf(ip,:) = v(:,ip)' - meanv(ip);
    wf(ip,:) = w(:,ip)' - meanw(ip);
end

% Calculate Urms, Vrms, and Wrms
uRMS = sqrt(sum(uf(2,:).^2)/ndata(ifile));
vRMS = sqrt(sum(vf(2,:).^2)/ndata(ifile));
wRMS = sqrt(sum(wf(2,:).^2)/ndata(ifile));

% Normalize to bow anemometer velocity
% uf=uf/Ubow
% vf=vf/Ubow
% wf=wf/Ubow

npdf = zeros(nprobe(ifile),1);
pdf = zeros(nprobe(ifile),2*nt+1,2*nt+1);
jpdf = zeros(nprobe(ifile),2*nt+1,2*nt+1);
for ip=1:nprobe(ifile)
    for i = 1:nbin
        for k = ibegin(i):iend(i)
            iu = floor(uf(ip,k)/du + 0.5) + nt + 1;
            iw = floor(wf(ip,k)/dw + 0.5) + nt + 1;
%            iu = floor(uf(ip,k)/Ubow/du + 0.5) + nt + 1;
```

```
%                iw = floor(wf(ip,k)/Ubow/dw + 0.5) + nt + 1;
                if (iu > 0) && (iu <= 2*nt+1) && (iw > 0) && (iw <= 2*nt+1)
                    npdf(ip) = npdf(ip)+1;
                    pdf(ip,iu,iw) = pdf(ip,iu,iw) + 1;
                    jpdf(ip,iu,iw)= jpdf(ip,iu,iw) - ((iu-nt-1)*du)*((iw-nt-
1)*dw);
                end
            end
        end
        pdf(ip,:,:) = pdf(ip,:,:)/npdf(ip)/du/dw;   %normalize
        jpdf(ip,:,:) = jpdf(ip,:,:)/npdf(ip)/du/dw;   %normalize
end

%% Run JPDF for no fenec data

% Num files for no fence data
nfile=66;

% Get file info
[loc nprobeNF ndata cont temp press
humid]=read_logc_file(pathNF,projectNF,beta,nfile);

[u v w
T]=PFC_read_velocity_data_file(pathNF,projectNF,beta,ifileNF,ndata(ifileNF),n
probeNF(ifileNF));

%[yaw,pitch] = yaw_pitch_angle(ndata,u,v,w);

[nbin ibegin iend
nvalid]=find_valid_data_chunks(1,yaw,ifileNF,ndata(ifileNF),u,v,w);

%running_average(yaw,ndata,nprobeNF,ifileNF,u,v,w,nbin,ibegin,iend)

[meanu(1:nprobeNF(ifileNF)),meanv(1:nprobeNF(ifileNF)),meanw(1:nprobeNF(ifile
NF)),uu(1:nprobeNF(ifileNF)),vv(1:nprobeNF(ifileNF)),ww(1:nprobeNF(ifileNF)),
uv(1:nprobeNF(ifileNF)),vw(1:nprobeNF(ifileNF)),wu(1:nprobeNF(ifileNF)),ke(1:
nprobeNF(ifileNF)),Su(1:nprobeNF(ifileNF)),Sv(1:nprobeNF(ifileNF)),Sw(1:nprob
eNF(ifileNF)),Fu(1:nprobeNF(ifileNF)),Fv(1:nprobeNF(ifileNF)),Fw(1:nprobeNF(i
fileNF))]=moment_valid(ndata(ifileNF),nprobeNF(ifileNF),nbin,ibegin,iend,u,v,
w);

Ubow = meanu(1);

% Find velocity fluctuations
uf = zeros(nprobeNF(ifileNF),length(u));
vf = zeros(nprobeNF(ifileNF),length(v));
wf = zeros(nprobeNF(ifileNF),length(w));
for ip=1:nprobeNF(ifileNF)
    uf(ip,:) = u(:,ip)' - meanu(ip);
    vf(ip,:) = v(:,ip)' - meanv(ip);
    wf(ip,:) = w(:,ip)' - meanw(ip);
```

```matlab
end

% Calculate Urms, Vrms, and Wrms
uRMS = sqrt(sum(uf(2,:).^2)/ndata(ifileNF));
vRMS = sqrt(sum(vf(2,:).^2)/ndata(ifileNF));
wRMS = sqrt(sum(wf(2,:).^2)/ndata(ifileNF));

% Normalize to bow anemometer velocity
% uf=uf/Ubow
% vf=vf/Ubow
% wf=wf/Ubow

npdfNF = zeros(nprobeNF(ifileNF),1);
pdfNF = zeros(nprobeNF(ifileNF),2*nt+1,2*nt+1);
jpdfNF = zeros(nprobeNF(ifileNF),2*nt+1,2*nt+1);
for ip=1:nprobeNF(ifileNF)
    for i = 1:nbin
        for k = ibegin(i):iend(i)
            iu = floor(uf(ip,k)/du + 0.5) + nt + 1;
            iw = floor(wf(ip,k)/dw + 0.5) + nt + 1;
%             iu = floor(uf(ip,k)/Ubow/du + 0.5) + nt + 1;
%             iw = floor(wf(ip,k)/Ubow/dw + 0.5) + nt + 1;
            if (iu > 0) && (iu <= 2*nt+1) && (iw > 0) && (iw <= 2*nt+1)
                npdfNF(ip) = npdfNF(ip)+1;
                pdfNF(ip,iu,iw) = pdfNF(ip,iu,iw) + 1;
                jpdfNF(ip,iu,iw)= jpdfNF(ip,iu,iw) - ((iu-nt-1)*du)*((iw-nt-
1)*dw);
            end
        end
    end
    pdfNF(ip,:,:) = pdfNF(ip,:,:)/npdfNF(ip)/du/dw;   %normalize
    jpdfNF(ip,:,:) = jpdfNF(ip,:,:)/npdfNF(ip)/du/dw;   %normalize
end

%% Plot pdf and jpdf

uRange = linspace(-nt*du,nt*du,2*nt+1);
wRange = linspace(-nt*dw,nt*dw,2*nt+1);

pdfPlot = zeros(2*nt+1,2*nt+1);
jpdfPlot = zeros(2*nt+1,2*nt+1);
jpdfSum = zeros(nprobe(ifile),1);
pdfPlotNF = zeros(2*nt+1,2*nt+1);
jpdfPlotNF = zeros(2*nt+1,2*nt+1);
jpdfSumNF = zeros(nprobeNF(ifileNF),1);
for n = 1:nprobe(ifile)
    for w = 1:nt*2+1
        pdfPlot(w,:,n) = pdf(n,:,w);
        jpdfPlot(w,:,n) = jpdf(n,:,w);
        jpdfSum(n,1) = jpdfSum(n,1) + sum(jpdf(n,:,w)*du*dw);
    end
end
```

```matlab
for n = 1:nprobeNF(ifileNF)
    for w = 1:nt*2+1
        pdfPlotNF(w,:,n) = pdfNF(n,:,w);
        jpdfPlotNF(w,:,n) = jpdfNF(n,:,w);

        jpdfSumNF(n,1) = jpdfSumNF(n,1) + sum(jpdfNF(n,:,w)*du*dw);
    end
end

x = -2:0.01:2;
y = -1:0.01:1;
figure(1),clf
set(gcf,'color','w')
hold on
contour(uRange,wRange,pdfPlot(:,:,probe))
plot(x,0,'k')
plot(0,y,'k')
xlabel('u'),ylabel('w')
axis([-2 2 -1 1])

x = -2:0.01:2.25;
y = -1.75:0.01:1.75;
figure(2),clf
set(gcf,'color','w')
hold on
[C,h] = contour(uRange,wRange,pdfPlotNF(:,:,probeNF));
clabel(C,h);
plot(x,0,'k')
plot(0,y,'k')
xlabel('u'),ylabel('w')
axis([-2 2 -1 1])

x = -2.75:0.01:2.5;
y = -2:0.01:2.25;
V = [-0.02, 0.02, 0.04, 0.06, 0.08, 0.1, 0.15];
figure(3),clf
set(gcf,'color','w')
hold on
[C,h] = contour(uRange,wRange,jpdfPlot(:,:,probe),V);
clabel(C,h);
plot(x,0,'k')
plot(0,y,'k')
xlabel('u'),ylabel('w')
axis tight
axis([-2 2.25 -1.75 1.75])

figure(4),clf
set(gcf,'color','w')
hold on
[C,h] = contour(uRange,wRange,jpdfPlotNF(:,:,probeNF),V);
clabel(C,h);
```

```matlab
plot(x,0,'k')
plot(0,y,'k')
xlabel('u'),ylabel('w')
axis tight
axis([-2 2.25 -1.75 1.75])

%% Plot JPDF
x = -3:0.01:3;
y = -2.5:0.01:2.5;
figure(5),clf
set(gcf,'color','w')
hold on
[C,h] = contour(uRange,wRange,jpdfPlot(:,:,probe),V,'b');
clabel(C,h,[-0.02, 0.02, 0.06, 0.1]);
[CNF,hNF] = contour(uRange,wRange,jpdfPlotNF(:,:,probeNF),V,'--r');
clabel(CNF,hNF,[-0.02, 0.02, 0.06, 0.1]);
plot(x,0,'k')
plot(0,y,'k')
legend('Fence','No Fence','Location','EastOutside')
xlabel('u'),ylabel('w')
axis tight
axis([-2.75 2.75 -2.1 2.1])
```

Energy Spectrum Creator (PFC_espectrum.m)

```matlab
%*********************************************************************
%                                                                   *
%        Program to obtain energy spectrum using SAW underway data  *
%            using sonic anemometers.                               *
%                                                                   *
%        The incoming wind direction from the starboard is          *
%            'negative' beta according to the coordinate system     *
%                                                                   *
%                              Hyung Suk Kang                       *
%                              2010. 10. 28                         *
%*********************************************************************
% E11: logitudinal energy spectrum for streamwise vel. comp.
% E22: logitudinal energy spectrum for cross-streamwise vel. comp.
% E33: logitudinal energy spectrum for wall-normal vel. comp.
clc; clear; close all;

% Parameters.
ndim=3;
H=59*0.0254;    %Deck height 59"
figure_on='T';  %plot
freq_Anem=20.;  %Anemometer sampling freq. 20Hz
nfft_Anem=2^9;
% freq_IMU=100.;   %IMU
% nfft_IMU=2^12; %2^12;
ifstart=52;     %file start number
ifend=52;       %file end number
probe = 3;      %set anemometer of interest

% Set path to find velocity file
energyPath = 'C:\LaSalle Trident\Underways\Fence\beta000\';

% Set project - Use PFC for fence data, SAW for no fence data
project = 'PFC';p=0;
%project = 'SAW';p=1;

% Set beta angle
yaw = '000';
beta= 000;

%% Select a yaw angle or incident angle and # files
```

```matlab
% Select yaw
% yaws = {'0 deg', '15 deg', '30 deg', '45 deg', '90 deg'};
% iyaw = menu('Select a yaw angle:', yaws);
% syaw = yaws{iyaw}; % string for yaw
% disp(['Yaw angle: ' syaw]);
%
% % Rip out the number from the text string
% syaw = syaw(isstrprop(syaw, 'digit'));
% yaw = -str2double(syaw); %should be - in yaw.

% # files for each yaw angle
if p == 0
    if (beta==0),   nfile=54; end
    if (beta==-15), nfile=23; end
    if (beta==-30), nfile=0; end
    if (beta==-90), nfile=0; end
elseif p == 1
    if (beta==0),   nfile=66; end
    if (beta==-15), nfile=39; end
    if (beta==-30), nfile=0; end
    if (beta==-90), nfile=0; end
end

% beta=0; nfile=62;
% beta=-15; nfile=37;
% beta=-30; nfile=5;
% beta=-90; nfile=5;

%% Read logc file.
[loc nprobe ndata cont temp press humid
time_be]=read_logc_file(energyPath,project,yaw,nfile);
loc=loc/H;

% Energy spectra: E11, E22 & E33
% for i=1:nfile
for i=ifstart:ifend
    disp('--------------------------------------------------');

    % Read velocity data file
    [u v w
T]=PFC_read_velocity_data_file(energyPath,project,yaw,i,ndata(i),nprobe(i));
%read data

    % Find the valid data chuncks
    [nbin ibegin iend
nvalid]=find_valid_data_chunks(1,beta,i,ndata(i),u,v,w);

    % Calculate statistics
    [meanu,meanv,meanw,uu,vv,ww,uv,vw,wu,ke,Su,Sv,Sw,Fu,Fv,Fw]=...
        moment_valid(ndata(i),nprobe(i),nbin,ibegin,iend,u,v,w);
```

```matlab
    % Coordinate transform to streamwise (u1), cross-streamwise (u2), wall
    % normal (u3) coordinate system from the ship reference coordinate system
(u, v, w).
    u1 = zeros(nvalid,nprobe(i));
    u2 = zeros(nvalid,nprobe(i));
    u3 = zeros(nvalid,nprobe(i));
    temp = 1;
    for j = 1:nbin
        for k = ibegin(j):iend(j)
            u1(temp,:) =  u(k,:)*cosd(beta) + v(k,:)*sind(beta);
            u2(temp,:) = -u(k,:)*sind(beta) + v(k,:)*cosd(beta);
            u3(temp,:) =  w(k,:);
            temp = temp + 1;
        end
    end

    % Energy spectrum for bow anemometer regardless of the incoming angle.
    vel_mag = meanu(1)*cosd(beta)+meanv(1)*sind(beta);

    % Normalize data
    u1 = u1/vel_mag;
    u2 = u2/vel_mag;
    u3 = u3/vel_mag;

    [E11]=energy_spectrum(u1(:,probe),nvalid,nfft_Anem);
    [E22]=energy_spectrum(u2(:,probe),nvalid,nfft_Anem);
    [E33]=energy_spectrum(u3(:,probe),nvalid,nfft_Anem);

    % Normalization
    delk=2.*pi/(vel_mag/freq_Anem*nfft_Anem);
    delf=freq_Anem/double(nfft_Anem);
    E11_f=E11/delf;
    E22_f=E22/delf*3./4.;
    E33_f=E33/delf*3./4.;
    E11  =E11/delk/(vel_mag^2*H);         % Normalization with U^2H
    E22  =E22/delk/(vel_mag^2*H)*3./4.;
    E33  =E33/delk/(vel_mag^2*H)*3./4.;
%     E11=E11/delk;
%     E22=E22/delk*3./4.;
%     E33=E33/delk*3./4.;


    % wavenumber and frequency
    kappa=    zeros(nfft_Anem/2+1,1);
    frequency=zeros(nfft_Anem/2+1,1);
    for j=2:nfft_Anem/2+1
        kappa(j)=    double(j-1)*delk*H;
        frequency(j)=double(j-1)*delf;
    end

    % Define frequency & nfft
    nfft=nfft_Anem;
```

```matlab
        freq=freq_Anem;

        % plots for wavenumber and frequency
        if (strcmpi(figure_on,'T'))
            figure(300+i);
            subplot(2,1,1);
            loglog(kappa(2:nfft/2+1),E11(2:nfft/2+1),'b'); hold on;
            loglog(kappa(2:nfft/2+1),E22(2:nfft/2+1),'r'); hold on;
            loglog(kappa(2:nfft/2+1),E33(2:nfft/2+1),'g'); hold on;
            xlabel('\kappa_1 H')
            ylabel('E_{11}, \frac{3}{4}E_{22} and \frac{3}{4}E_{33}')
%           xlim([0 ndata]);
%           ylim([min(u(:,nBow)) max(u(:,nBow))]);
            title('Eii');

            subplot(2,1,2);
            loglog(frequency(2:nfft/2+1),E11_f(2:nfft/2+1),'b'); hold on;
            loglog(frequency(2:nfft/2+1),E22_f(2:nfft/2+1),'r'); hold on;
            loglog(frequency(2:nfft/2+1),E33_f(2:nfft/2+1),'g'); hold on;
%           xlim([0 ndata]);
%           ylim([min(u(:,nBow)) max(u(:,nBow))]);
            title('Eii in frequency domain');
        end

        % Wright Tecplot data file.
        str1=num2str(abs(beta),'%03d');
        str2=num2str(i,'  %03d');
        if(beta<=0), file_out=['./Eii-yaw',str1,'-',str2,'.dat']; end
        if(beta>0),  file_out=['./Eii+yaw',str1,'-',str2,'.dat']; end
        fid6=fopen(file_out,'w');

        fprintf(fid6, 'TITLE="Eii"\r\n');
        fprintf(fid6,
'variables="kH","nE11","nE22","nE33","freq","E11_f","E22_f","E33_f"\r\n');
        fprintf(fid6, 'zone I=%d, F=point\r\n',nfft/2);

        for k=2:nfft/2+1
            fprintf(fid6,'%12.5e %12.5e %12.5e %12.5e %12.5e %12.5e %12.5e
%12.5e\r\n',...

kappa(k),E11(k),E22(k),E33(k),frequency(k),E11_f(k),E22_f(k),E33_f(k));
        end
        fclose(fid6);

end
```